X. OPTICAL AND INFRARED SPECTROSCOPY*

Academic and Research Staff

Prof. C. H. Perry
Dr. R. P. Lowndes

Graduate Students

Jeanne H. Fertel
J. F. Parrish
N. E. Tornberg

RESEARCH OBJECTIVES AND SUMMARY OF RESEARCH

The principal investigator transferred to Northeastern University, Boston, Massachusetts, in September 1968. The experimental study of solids by infrared and Raman techniques was discontinued at that time, but several research programs have been completed and the data have been analyzed. Four of these studies are reported in Sections X-A, X-B, X-C, and X-D. The results of the remaining studies will be included in a future report.

Work on thallium and silver halides, alkaline-earth fluorides, and potassium tantalate-niobate mixed crystals continues. Six journal papers are in preparation which will essentially cover most of the unpublished work completed at M. I. T. Three graduate students will be candidates for the Ph. D. degree in January 1969.

In addition to the work reported here, the publications and papers presented at various meetings summarize the research accomplished during the past year.[1-7]

C. H. Perry

References

1. R. P. Lowndes, J. F. Parrish, and C. H. Perry, "Optical Phonons in Tysonite Rare-Earth Fluorides," Paper L-1. Symposium on Molecular Structure and Spectroscopy, Ohio State University, Columbus, Ohio, September 3-7, 1968.
2. J. F. Parrish, R. P. Lowndes, and C. H. Perry, "Far Infrared Electronic Transitions in Tysonite Rare-Earth Fluorides," Paper L-2. Symposium on Molecular Structure and Spectroscopy, Ohio State University, Columbus, Ohio, September 3-7, 1968.
3. Jeanne H. Fertel, K. Owyang, and C. H. Perry, "Observation of Two-Mode Behavior in an Alkali Halide Mixed-Crystal System," Paper L-3. Symposium on Molecular Structure and Spectroscopy, Ohio State University, Columbus, Ohio, September 3-7, 1968.
4. R. P. Lowndes and D. H. Martin, "Temperature Dependence under Constant Volume of Lattice Resonance in Ionic Solids," Paper L-4. Symposium on Molecular Structure and Spectroscopy, Ohio State University, Columbus, Ohio, September 3-7, 1968.
5. C. H. Perry and N. E. Tornberg, "The Temperature-Dependent Phonon Spectrum of $PbTiO_3$," Paper L-5. Symposium on Molecular Structure and Spectroscopy, Ohio State University, Columbus, Ohio, September 3-7, 1968.

*This work was supported in part by the Joint Services Electronics Programs (U. S. Army, U. S. Navy, and U. S. Air Force) under Contract DA 28-043-AMC-02536(E), the National Aeronautics and Space Administration (Grant NGR-22-009-237), and the U. S. Air Force Cambridge Research Laboratories Contract AF 19(628)-6066.

6. N. E. Tornberg and C. H. Perry, "The Phonon Spectra and Phase Transitions in the K(Ta:Nb)O_3 Mixed-Crystal System," Paper L-6. Symposium on Molecular Structure and Spectroscopy, Ohio State University, Columbus, Ohio, September 3-7, 1968.

7. C. H. Perry and N. E. Tornberg, "Raman Spectra of $PbTiO_3$ and Solid Solutions of $NaTaO_3$-$KTaO_3$ and $KTaO_3$-$KNbO_3$," Paper F-3. International Conference on Light-Scattering Spectra of Solids, New York University, New York, September 3-6, 1968 (in Proceedings, W. G. Wright (ed.), Springer-Verlag, New York, 1969).

A. OPTICAL PHONONS AND SYMMETRY OF TYSONITE LANTHANIDE FLUORIDES

1. Introduction

The partially filled 4f electron shell of the lanthanide elements is so well screened from its external environment that, when the ions are held in a suitable host lattice, electronic transitions of the type 4f → 4f are expected to give sharp spectral lines. Some of the known 4f → 4f transitions lie in the far infrared region of the spectrum.[1-5] Consequently, there is strong motivation to assess the potential of these low-energy transitions for use in solid-state, far infrared lasers.

It is clear, however, that in order to investigate these potential far infrared lasing systems, the host lattice must be chosen with care. This is true not only because the host lattice will determine the position and line width of the 4f → 4f transitions but also because the optically active phonon frequencies of most solids lie within the far infrared region too, and precautions should be taken to ensure that the frequencies of the electronic and phonon excitations do not significantly overlap.

The tysonite structure of LaF_3, CeF_3, PrF_3, and NdF_3 provides a convenient host lattice in which other lanthanide ions will enter substitutionally. These substances are rugged[6,7] and readily available in single crystal form.[8,9] Their nonhygroscopic nature[6,7] has the spectroscopic advantage that they are unlikely to incorporate OH^- impurities, which are well known to contribute defect modes to the phonon spectrum of a host lattice.[10]

X-ray diffraction studies have led to three commonly proposed lattices for the tysonite structure: a hexamolecular cell with $P6_3/mcm$ $\left(D_{6h}^3\right)$ symmetry,[11,12] a bimolecular cell with $P6_3/mmc$ $\left(D_{6h}^4\right)$ symmetry,[13] and a hexamolecular cell with $P\bar{3}c1$ $\left(D_{3d}^4\right)$ symmetry.[14-16] Faraday or paramagnetic rotation,[17,18] electron spin resonance,[19-21] and optical absorption measurements[1-4,22-29] have provided a substantial amount of additional experimental evidence, but the proper space group for the tysonite structure has not yet been conclusively established. In fact, some of the magnetic resonance

data[19, 20] appear inconsistent with all three of these lattices. Recently, Baumann and Porto[5] reported the frequencies and polarizations of the Raman active phonon modes for these four tysonite lanthanide fluorides. Their results, for LaF_3 at least, strongly favor the hexamolecular $P\bar{3}c1$ lattice.

The frequencies and polarizations of the fundamental infrared active phonon modes, for the most part, are not known for these compounds, although some attempts have been made to determine them for LaF_3 from transmission measurements on polycrystalline samples[30] and from unpolarized emittance spectra.[31] Since the lanthanide fluorides are uniaxial, however, the dielectric response tensor contains two principal nondegenerate components, and the infrared active modes can only be measured uniquely by using radiation polarized separately along these two orthogonal components. Consequently, these previous experiments have not necessarily identified all of the fundamental phonon transitions.

This report complements the recent Raman study[5] and presents a complete set of polarized, fundamental, infrared active phonon modes for LaF_3, CeF_3, PrF_3, and NdF_3 at temperatures between 7°K and 295°K. These infrared results for the tysonite lattice, together with the Raman results, are consistent only with the $P\bar{3}c1$ $\left(D_{3d}^4\right)$ lattice containing 6 formula units per unit cell and conclusively eliminate the $P6_3/mcm$ and $P6_3/mmc$ lattices. In order to be consistent with the magnetic-resonance data, the proper magnetic space group must be $P\bar{3}'c'1$.

2. Experimental Details

Cylindrical single crystals of LaF_3, CeF_3, PrF_3, and NdF_3, 10 mm in diameter and approximately 5 mm long, were obtained from Optovac, Inc.[8] The crystals were supplied with the c-axis perpendicular to the cylinder axis and parallel to the plane of the circular end faces. By using crossed polarizers, the c axis could be oriented with respect to the polarization of the incident radiation to better than 5 degrees of arc; this resulted in an intermixing between the orthogonal polarizations of less than 2% reflectance. Only the CeF_3 sample showed the hexagonal striations reported to be associated with oxygen impurities.[6]

The reflectance and transmittance spectra were measured with an R.I.I.C. FS-520 Fourier spectrometer (Michelson type) adapted for 12-bit analog-to-digital conversion. A mercury arc source in conjunction with a liquid-helium-cooled Ga doped germanium bolometer was used from 40-200 cm^{-1}. A Nernst glower with a Golay pneumatic cell was used from 150-650 cm^{-1}. A vacuum-evaporated one-dimensional wire grid polarizer was used to reduce the horizontally polarized radiation to much less than 1% of the vertically polarized component.[32]

The normalized transmittance was calculated with the use of an aperture that had the

same size as the sample. The normalized reflectance was calculated with the use of an aluminum mirror as a reference background. The plane of incidence was horizontal and the angle of incidence was approximately 7 1/2 degrees of arc. By orienting the crystal so that the c axis lay in the face of the crystal and was either vertical or horizontal, either the π component (E//c) or the σ component (E$\perp$c) of the dielectric response tensor could be individually excited.

3. Dielectric Response Tensor

The effective dielectric response function for each tensor component was calculated from a Kramers-Kronig analysis of the reflectance measurements by using the Fresnel formula that is appropriate for a crystal aligned with the desired axis precisely parallel to the incident electric field and perpendicular to the plane of incidence. The infrared active transverse optical (TO) frequencies, associated with the poles of the dielectric response function ($|D| \neq 0$, $|E| \to 0$), were located by peaks in $\omega\epsilon''$ ($\hat{\epsilon} = \epsilon' + i\epsilon''$), which is proportional to the electric conductivity $\sigma = \frac{\omega\epsilon''}{4\pi}$. The infrared active longitudinal optical (LO) frequencies, associated with the zeros of the dielectric response function ($|D| \to 0$, $|E| = 0$),[33] were located by peaks in $-\omega\eta''$ ($\hat{\epsilon}^{-1} = \hat{\eta} = \eta' + i\eta''$, $\eta'' = -\epsilon''/|\hat{\epsilon}|$).

The principal poles and zeros of the two components of the dielectric response tensor were identified quite satisfactorily by using the outlined procedure. There were, however, measurable effects in both reflectance and transmittance because of a slight misalignment of the crystal axes. In order to understand the nature and magnitude of the effects of this misalignment, it is instructive to solve a special case of the reflectance and transmittance of a uniaxial crystal.

In a uniaxial crystal ($\epsilon_x = \epsilon_y \neq \epsilon_z$), the incident radiation splits into an ordinary wave and an extraordinary wave that propagate independently of one another. If the direction of propagation of the incident radiation is normal to the crystal-vacuum interface, the ordinary and extraordinary waves propagate in the same direction as the incident radiation. If ϕ is the angle between the incident electric field and the projection of the c axis on the crystal face, it can be shown that $R = R_o \sin^2 \phi + R_e \cos^2 \phi$ and $T = T_o \sin^2 \phi + T_e \cos^2 \phi$, where R and T are the effective normal reflectance and transmittance coefficients of the crystal, R_o, T_o, R_e, and T_e are the normal reflectance and transmittance coefficients for the ordinary and extraordinary waves, respectively.

If $\phi \approx 0$, then $R = R_e + (R_o - R_e) \sin^2 \phi \approx R_e$. Since $|R_o - R_e| \leq 1$ and, in practice, $\sin^2 \phi \leq 0.01$, it is clear that one can measure the extraordinary reflectance coefficient within an additive error of less than 1% reflectance. Similarly, if $\phi \approx 90°$, the ordinary reflectance coefficient can be measured within 1% reflectance. As a result, the errors introduced in the measurement of the reflectance or transmittance by a slight error (less than 5 degrees of arc) in the orientation of the plane of polarization with respect to the

optical axis can either be conveniently ignored or be eliminated by small corrections based upon measurements in the orthogonal plane of polarization.

Moreover, since $R_o = \left|(1-\hat{n}_x)/(1+\hat{n}_x)\right|^2$ and we ignore interference effects, $T_o \approx (1-R_o)^2 \exp[-\alpha_x d]$, where $\hat{n}_x = (\mu\epsilon_x)^{1/2}$, d ≡ thickness of the crystal, and $\alpha_x = 2\pi\omega \text{ Im } [\hat{n}_x]$, one of the components of the dielectric response tensor, ϵ_x, can be calculated directly from R_o and T_o.

Unfortunately, ϵ_z cannot be calculated directly from R_e and T_e. $R_e = \left|(1-\hat{n}_e)/(1+\hat{n}_e)\right|^2$, with interference effects $T_e \approx (1-R_e)^2 \exp[-\alpha_e d]$ ignored, where $\hat{n}_e = c/v_e$ and $\alpha_e = 2\pi\omega \text{ Im } (\hat{n}_e)$, but $v_e^2 = v_z^2 \cos^2\theta + v_x^2 \sin^2\theta$, where $v_x^2 = c^2/\mu\hat{\epsilon}_x$, $v_z^2 = c^2/\mu\hat{\epsilon}_z$, and θ is the angle between the c axis and the plane of the crystal face.

The crystals used in this study were cut and polished with the c axis parallel to the face of the crystal within an estimated 5 degrees of arc, so that $\sin^2\theta \approx \theta^2 \leq 0.01$, and $v_e^2 \approx v_z^2 + \left(v_x^2 - v_z^2\right)\theta^2$. Equivalently, $\hat{n}_e \approx \hat{n}_z \left(1 + \theta^2\left(\frac{\epsilon_z}{\epsilon_x} - 1\right)\right)^{-1/2} \approx \hat{n}_z - \frac{\theta^2}{2\epsilon_x}\hat{n}_z(\epsilon_z - \epsilon_x)$, as long as $\left|\theta^2/\epsilon_x\right| \ll 1$. Under these conditions $R_e \approx R_z \pm 2\theta^2 R_z \left|\frac{\hat{n}_z}{1-\epsilon_z}\right| \cdot \left|\frac{\epsilon_z - \epsilon_x}{\epsilon_x}\right|$, and $T_e \approx (1-R_e)^2 \exp(-\alpha_e d)$, where $R_z = \left|(1-\hat{n}_z)/(1+\hat{n}_z)\right|^2$, $\alpha_e \approx \alpha_z - \pi\omega \text{ Im } \left[\frac{\theta^2}{\epsilon_x}\hat{n}_z(\epsilon_z - \epsilon_x)\right]$, $\hat{n}_z = (\mu\epsilon_z)^{1/2}$, and $\alpha_z = 2\pi\omega \text{ Im } [\hat{n}_z]$.

Clearly, even when $\theta^2 \leq 0.01$, there is no assurance that the difference between R_e and R_z and between T_e and T_z must be less than 1%. In fact, whenever $|\epsilon_x| \to 0$, that is, whenever one is near a pole of $\eta_z = \epsilon_x^{-1}$, significant features may be expected in R_e and T_e. In a low-dispersion region of ϵ_z in with Re $[\hat{n}_z] \approx$ const $= n_z$ and Im $[\hat{n}_z] \to 0$, then $R_e \approx R_z + K_1 \frac{\theta^2}{|\epsilon_x|}$ and $\alpha_e \approx -K_2\theta^2\omega\eta_x''$, where $\eta_x'' = \text{Im}\left[\epsilon_x^{-1}\right]$, $K_2 = \pi n_z^3/\mu$, and K_1 may be evaluated from R_e and R_o. Consequently, even in regions where ϵ_z is approximately constant, there will be a weak peak in the reflectance and a moderately strong minimum in the transmittance that is proportional to θ^2 whenever the frequency approaches a longitudinal optical (LO) frequency of ϵ_x. Minima in the extraordinary transmittance near poles of $\hat{\eta}_z = \hat{\epsilon}_z^{-1}$, on account of the LO frequencies of ϵ_z, can also be observed for radiation propagating almost parallel to the optical axis.

This weak coupling of the nominally transverse material electromagnetic wave (mixed photon-phonon particle wave) to the longitudinal optical (LO) frequencies of the orthogonal components of the dielectric response tensor has not apparently been previously reported, although it is a general property of all strongly anisotropic ($|\hat{\epsilon}_x - \hat{\epsilon}_z| \gg 0$) transparent crystals. The existence of this effect makes it possible for some longitudinal dielectric resonances to be studied in transmission as if they were weak transverse resonances, as well as to identify intrinsic but otherwise spurious

absorption bands, because of a slight misalignment of an anisotropic crystal with strong longitudinal resonances.

An observation of the lowest LO frequency of the ϵ_x component of the tysonite lanthanide fluorides is reported below.

4. Experimental Results

Figure X-1 shows the measured specular reflectance of LaF_3, CeF_3, PrF_3, and NdF_3 at 7°K with E // c (π-polarized modes). Five infrared active phonon modes appear for LaF_3 and CeF_3, but for PrF_3 and NdF_3 there are 6 infrared active phonon modes. The sixth mode arises from the lifting of an apparent degeneracy of the reflection band at 220 cm^{-1}. For PrF_3 an additional band at 66 cm^{-1}, which is not present in the reflectance spectra of the other salts, is observed. This band is believed to be due to an electronic transition from the ground state to the first excited state of the $^3H_4$ Stark multiplet of Pr^{3+}. This transition has been predicted from optical absorption

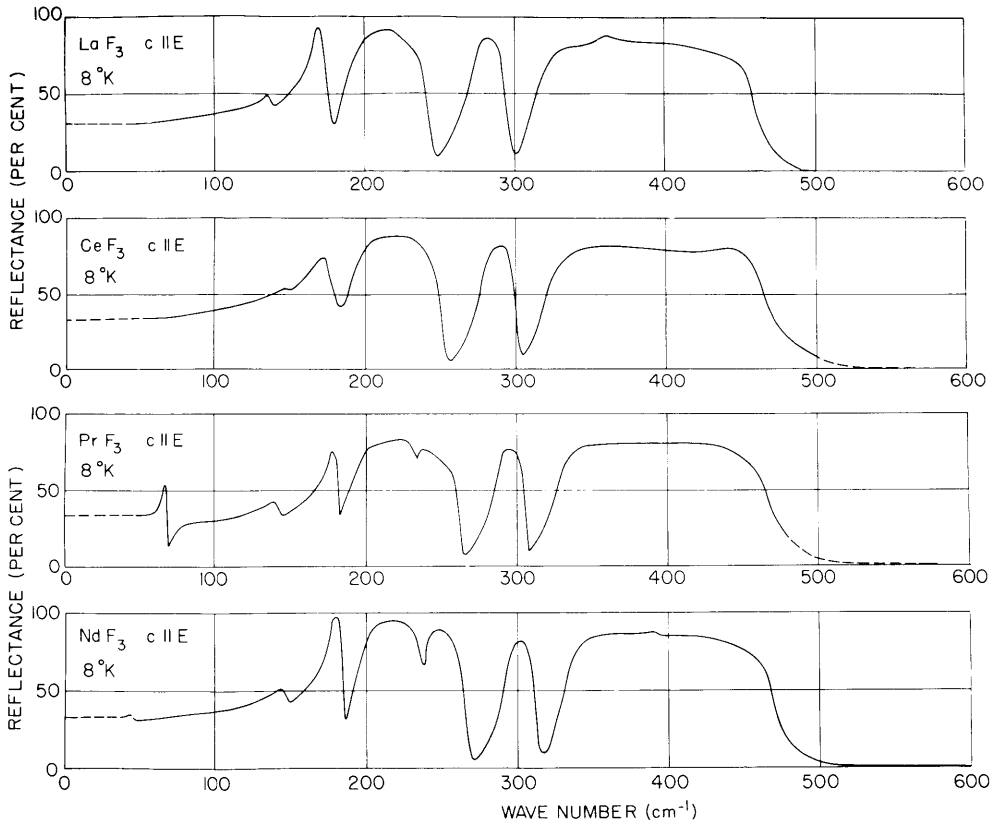

Fig. X-1. Far infrared reflectance of the lanthanide fluorides at 7°K in the π-polarization.

measurements[4, 22, 25-28] to occur near 66 cm^{-1}, and its nature has been confirmed on the basis of far infrared transmission measurements of Pr^{3+} contained within these four host lattices.[34] A perceptible change in the reflectance of NdF_3 was also observed in this polarization near 45 cm^{-1}, which was due to an electronic transition from the ground state to the first excited state of the $^4I_{9/2}$ Stark multiplet of the Nd^{3+} ion. This last transition has been confirmed, by Zeeman splitting,[34] to be electronic in nature.

Figure X-2 shows the measured spectral reflectance for the four salts at 7°K with $E \perp c$ (σ-polarized modes). In this polarization at least 10 well-defined infrared active phonon modes are observed, although the reflection band centered near 140 cm^{-1} in LaF_3 is only partially resolved in NdF_3. Proceeding through the series from LaF_3 through NdF_3, a moderately strong shoulder appears on the low-frequency side of the reflection band near 130 cm^{-1} (in LaF_3) and it is quite likely that, in fact, there are 11 infrared active phonon modes in the σ-polarization. For PrF_3, an additional reflection band (at 92 cm^{-1}) is again observed which is not present in the spectra of the other salts. This mode is believed to be due to an electronic transition from the ground state of the

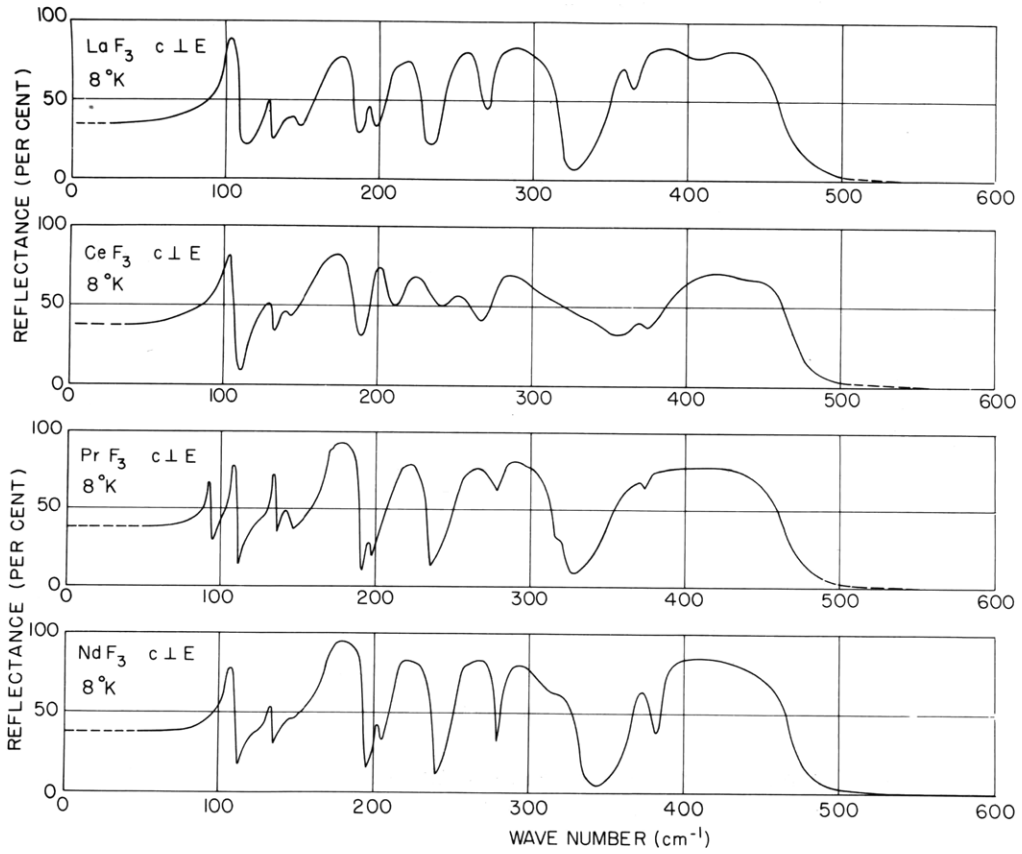

Fig. X-2. Far infrared reflectance of the lanthanide fluorides at 7°K in the σ-polarization.

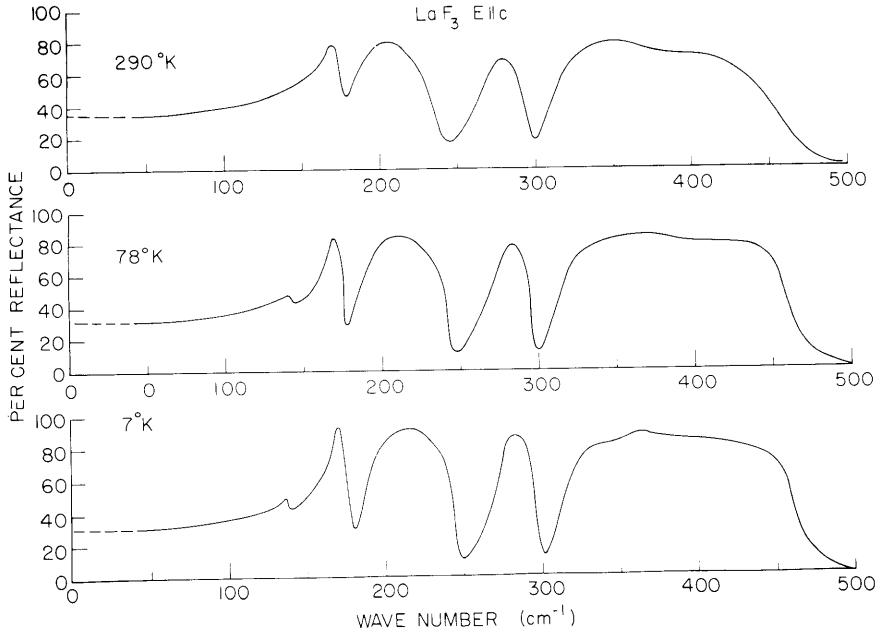

Fig. X-3. Temperature dependence of the far infrared reflectance of LaF_3 in the π-polarization.

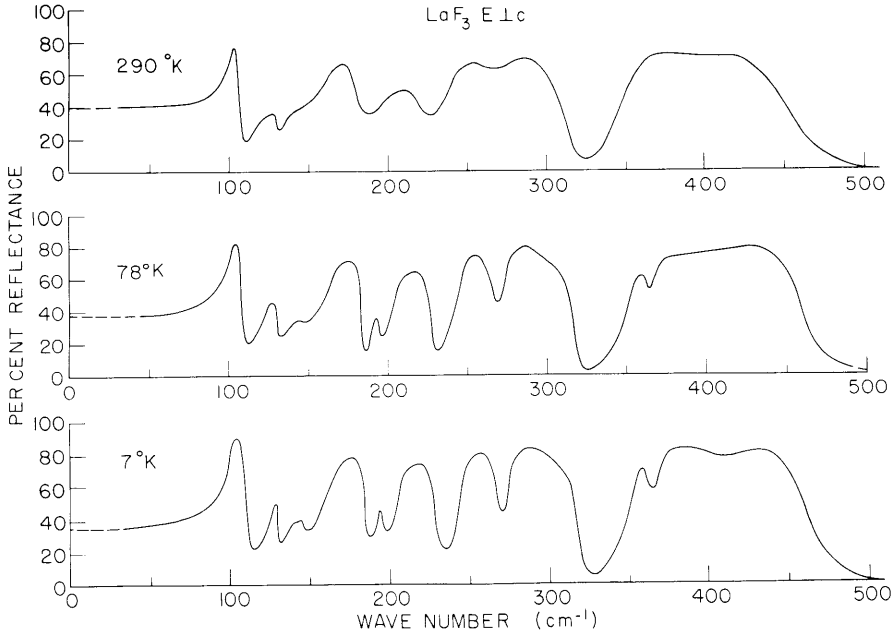

Fig. X-4. Temperature dependence of the far infrared reflectance of LaF_3 in the σ-polarization.

$^3H_4$ Stark multiplet of the Pr^{3+} ion to the second excited state, for the same reasons as those given above for the electronic transitions observed in the π-polarization.

Figures X-3 and X-4 illustrate the temperature dependence that is typical of the reflectance spectra in the π- and σ-polarizations for LaF_3 between 7°K and 295°K. It is evident that a fairly rapid damping of the weaker reflection bands occurs as the temperature is raised, so that at 295°K there are only 4 well-defined reflection bands in the π-polarization and 7 in the σ-polarization. The damping out of the weaker reflection bands is a continuous process with increasing temperature and there is no evidence for a phase change.

Kramers-Kronig analyses of the reflectance measurements determined the dielectric functions $\omega\epsilon''$ and $\omega\eta''$ for each lanthanide fluoride. Figure X-5 shows the typical shape of these functions for NdF_3. Six TO and LO frequencies can be easily distinguished in the π-polarization, but only 10 TO and LO frequencies can be easily seen in the

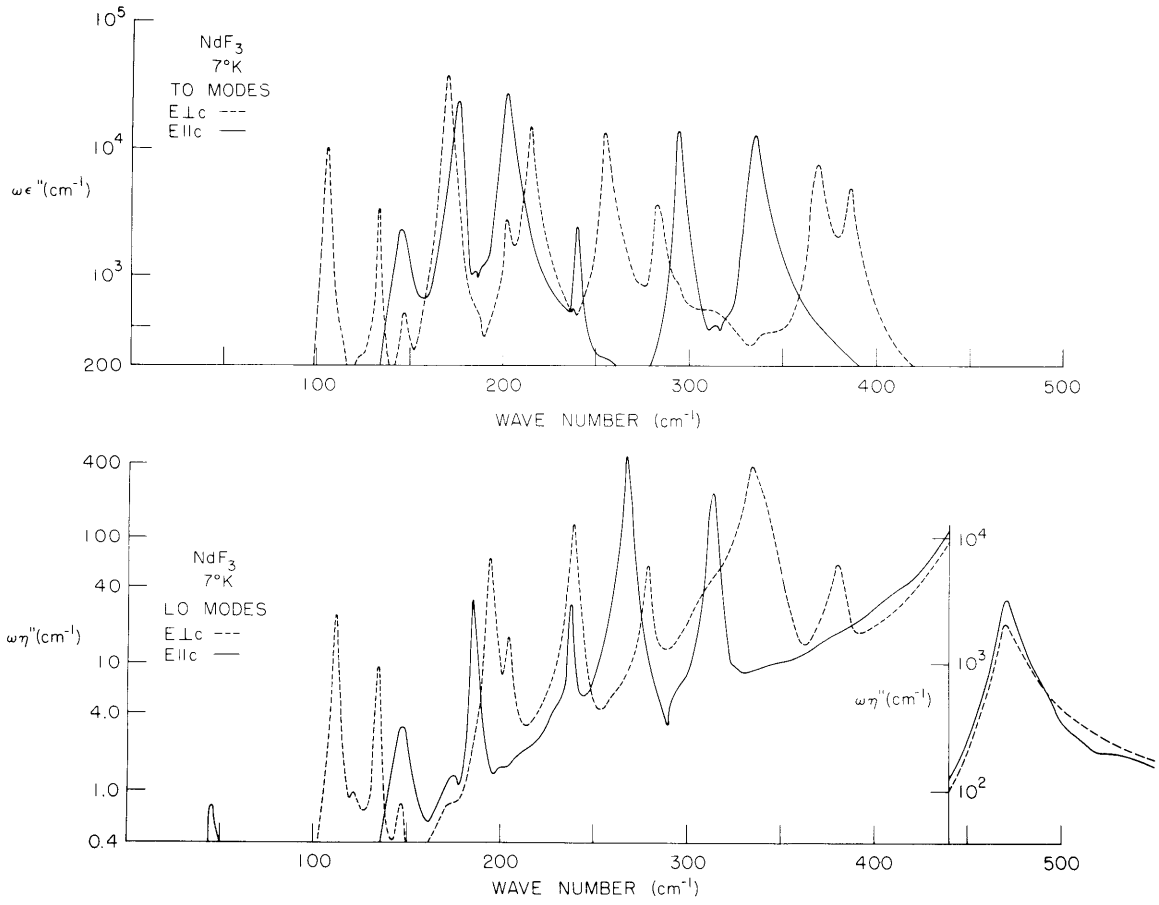

Fig. X-5. Frequency dependence of the dielectric functions $\omega\epsilon''$ and $\omega\eta''$ for NdF_3 at 7°K.

Table X-1. Transverse and longitudinal $k \approx 0$ phonon frequencies and their associated damping in cm^{-1} for the lanthanide fluorides in the π-polarization. The phonon frequencies are accurate to $\pm 2\ cm^{-1}$, and the damping to $\pm 20\%$.

	LaF_3			CeF_3			PrF_3			NdF_3		
^oK	5	78	295	5	78	295	5	78	295	5	78	295
ω_T	138	142		140	141		141	141		144	147	
γ_T	3	5		9	9		5	16		10		
ω_L	138	143		140	141		143	142		147	147	
γ_L	4	5		8	8		5	17		10		
ω_T	166	168	168	170	170	167	178	175	170	176	177	172
γ_T	4	4	6	5	6	10	3	9	16	5	4	8
ω_L	178	178	176	180	181	180	183	182	182	185	185	184
γ_L	3	4	7	6	10	20	2	6	15	3	3	12
ω_T	194	195	194	199	203	193	201	203	195	202	202	198
γ_T	8	9	14	8	11	24	10	17	20	6	7	15
ω_L	246	243	239	252	252	249	263	261	257	268	267	264
γ_L	5	7	16	8	8	16	6	7	20	4	6	14
ω_T							234	232		240	238	236
γ_T										3	6	
ω_L							234	232		238	236	234
γ_L										4	5	
ω_T	273	274	275	280	285	273	289	288	283	294	294	290
γ_T	8	10	12	3	6	20	6	8	20	4	6	17
ω_L	298	297	296	302	301	303	308	307	308	314	314	312
γ_L	6	6	10	4	7	13	5	4	20	5	6	14
ω_T	318	319	323	329	339	321	331	332	339	335	337	337
γ_T	14	14	16	6	14	18	8	15	20	8	8	12
ω_L	462	461	468	478	475	466	471	474	467	470	472	472
γ_L	14	18	62	23	38	17	15	20	20	13	18	44

Table X-2. Transverse and longitudinal $k \approx 0$ phonon frequencies and their associated damping in cm^{-1} for the lanthanide fluorides in the σ-polarization. The phonon frequencies are accurate to ± 2 cm^{-1}, and the damping to $\pm 20\%$.

	LaF_3			CeF_3			PrF_3			NdF_3		
^oK	5	78	295	5	78	295	5	78	295	5	78	295
ω_T	101	100	100	98	98	100	107	104	102	104	105	101
γ_T	2	7	5	6	6	7	3	4	6	3	6	8
ω_L	110	110	108	108	107	108	111	110	109	112	111	110
γ_L	4	7	4	5	4	4	3	4	6	3	4	5
ω_T	128	127	128	130	130	130	134	132	131	133	133	131
γ_T	3	8	8	4	4	7	2	5	13	3	4	
ω_L	130	131	130	132	132	132	136	135	133	135	135	136
γ_L	3	7	7	3	4	7	2	6	10	3	4	20
ω_T	144	144		142			142	143		147		
γ_T	11			5			8			6		
ω_L	146	145		142			145	143		147		
γ_L	11			2			8			6		
ω_T	168	167	168	164	166	164	169	170	166	170	170	165
γ_T	8	10	11	9	10	10	25	5	14	5	6	17
ω_L	184	184	183	186	186	186	189	169	190	194	194	193
γ_L	5	5	18	8	7		2	3	14	3	4	14
ω_T	193	193		198	201		196			204	202	
γ_T	10	7		6			4			4		
ω_L	196	195		210	208		197			204	202	
γ_L	10						3			5		
ω_T	210	208	208	218	222	203	213	211	205	215	214	208
γ_T	8	10	34				8	11		8	10	
ω_L	230	229	222	240	235	224	235	235	228	239	238	233
γ_L	8	10	26				4	12		6	8	
ω_T	246	248	245	247	247	244	255	252	248	255	255	251
γ_T	6	7	19				7	13	25	5	8	25
ω_L	268	268	272	264	266	272	278	276	278	279	279	278
γ_L	9	12					20			5	12	
ω_T	274	272	268	276	278	269	280	278	278	283	284	278
γ_T	8	13		20			10			5	11	
ω_L	318	317	316	350	350	318	323	322	324	334	334	332
γ_L	10	10	16			34	15	16	25	12	16	23
ω_T	356	354		364			354	355		369	368	366
γ_T	9	13					20	23		8	10	30
ω_L	364	364		374			373	373		381	381	
γ_L	15									10	12	
ω_T	368	367	356	382	385	360	374	375	358	386	385	370
γ_T			15			44	16	20	33	9		33
ω_L	466	462	457	472	474	478	468	464	467	471	471	463
γ_L	31	19	35	26	33	72	16	23	33	18	20	30

σ-polarization. A weak but sharp feature near 125 cm^{-1} in both $\omega\epsilon''$ and $\omega\eta''$ has been interpreted as an eleventh fundamental phonon mode, because of its appearance as a shoulder on the low-frequency side of another fundamental phonon mode and because it occurs at a frequency lower than expected for two-phonon summation processes. The weak broad feature near 320 cm^{-1}, which is even weaker than the mode near 125 cm^{-1}, has been interpreted as a two-phonon summation process because it is at a sufficiently high frequency and appears on the high-frequency side of a fundamental phonon mode. Tables X-1 and X-2 summarize the $k \approx 0$ infrared active transverse and longitudinal optical phonon frequencies and their associated half-widths as determined for each of the four lanthanide fluorides from the dielectric functions described above. These tables reveal that the frequency of any particular lattice mode in LaF_3 moves to higher frequencies as the reduced mass of the host lattice is increased. This reflects the stronger interatomic forces present in the heavier lattices as a result of the lanthanide contraction of the cell volume as the atomic number of the cation is increased.[35]

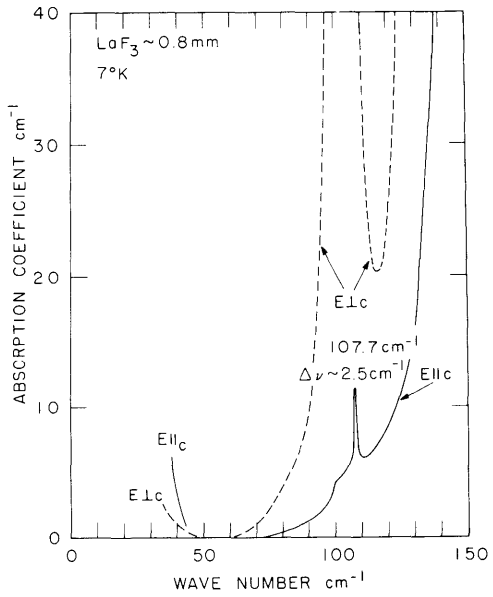

Fig. X-6. Frequency dependence of the absorption coefficient of LaF_3 at 7°K calculated from transmittance data.

Figure X-6 shows the frequency dependence of the absorption coefficient from 40-150 cm^{-1} for one sample of LaF_3 at 7°K in both orthogonal polarizations. In the σ-polarization, a strong band centered near 103 cm^{-1} dominates the spectrum, as predicted by the reflectance measurements. In the π-polarization, the weak band centered at 107.7 cm^{-1} with a half-width of approximately 2 cm^{-1} is interpreted as the $k \approx 0$ longitudinal optical phonon frequency forecast from the reflectance measurements to be between 109 and 110 cm^{-1} with a half-width of approximately 3 cm^{-1}. As we have explained, this weak absorption attributable to the longitudinal mode varies in strength

from sample to sample and is seen because the crystal c-axis was slightly misaligned from the E // c and k ⊥ c requirements for the π-polarization. The ratio of the reduced strength measured in transmission to the full strength measured in reflection suggests that the angle of misalignment for this sample was approximately 3 degrees of arc. The equivalent longitudinal mode was seen in transmittance at 108 cm^{-1} for CeF_3, 111 cm^{-1} for PrF_3, and 112 cm^{-1} for NdF_3.

On the basis of unpolarized emittance spectra, Rast et al.[31] have reported the $k \approx 0$ transverse optical phonon frequencies for k // c (equivalent to the σ-polarization) to be at 92, 100, 115, 128, 166, 192, 208, 246, 272, 353, and 368 cm^{-1}, and the additional frequencies of k ⊥ c (mixture of σ-polarization and π-polarization) to be at 170, 203, 235, 264, and 304 cm^{-1}. In the σ-polarization, the emittance frequencies, for the most part, are quite close to those determined from the reflectance data. The exceptions are that neither the 92 cm^{-1} nor the 115 cm^{-1} transitions seen in emittance are seen in either reflectance or transmittance measurements. Conversely, the emittance results show no sign of the phonon modes observed in reflectance just above and below the moderately strong band near 130 cm^{-1}. In the π-polarization, the emission frequencies are not in good agreement with those observed in reflection, except for the strong lattice mode at 170 cm^{-1}. This may be due to the fact that the emittance frequencies for the π-polarization were, in fact, recorded with k ⊥ c rather than with E // c, as was done in reflection. As a result, the emittance experiment simultaneously excited the infrared active modes in both orthogonal polarizations, thereby yielding a strongly mixed spectrum that is difficult to relate to the dielectric response function in either polarization.

5. Lattice Space Group

Table X-3 summarizes some results of group theoretical vibrational analysis for several structures proposed for the tysonite lattice from x-ray diffraction studies. From the low-temperature infrared measurements, the existence of 6 infrared active modes in the (z) polarization (E // c) and at least 10 (probably 11) infrared active modes in the (xy) polarization (E ⊥ c) can be inferred. Therefore, the $P6_3/mmc$ $\left(D_{6h}^{4}\right)$ lattice,[13] which predicts 2 (z) and 2 (xy) infrared active modes, and the $P6_3/mcm$ $\left(D_{6h}^{4}\right)$ lattice,[12] which predicts 4 (z) and 7(xy) infrared active modes can both be eliminated as possible tysonite lattices. The $P\bar{3}c1$ $\left(D_{3d}^{4}\right)$ lattice[14-16] and the $P6_322$ $\left(D_{6}^{6}\right)$ lattice[11] are both compatible with the infrared measurements. The $P6_322$ lattice can be eliminated, however, because it predicts almost twice as many doubly degenerate Raman active modes as observed,[5] and because it predicts that all eleven of the (xy) infrared active modes should also be Raman-active. Likewise, the noncentrosymmetric P3c1 lattice, which is consistent with the most recent x-ray studies,[14-16] can be eliminated by either

Table X-3. Optically active phonons in proposed tysonite lattices.

Lattice Space Group	Formula Units	Lanthanide Site Symmetry	Optical Activity*			
			1R-π	Raman-A	1R-σ	Raman-E
$P6_3/mmc$ (D^4_{6h})	2	$\bar{6}m2$ (D_{3h})	$2A_{2u}$	$1A_{1g}$	$2E_{1u}$	$1E_{1g}$ $3E_{2g}$
$P6_3/mcm$ (D^3_{6h})	6	mm (C_{2v})	$4A_{2u}$	$3A_{1g}$	$7E_{1u}$	$4E_{1g}$ $8E_{2g}$
$P\bar{3}c1$ (D^4_{3d})	6	2 (C_2)	$6A_{2u}$	$5A_{1g}$	$11E_u$	$12E_g$
$P6_322$ (D^6_6)	6	2 (C_2)	$6A_2$	$5A_1$	$11E_1$	$11E_1$ $12E_2$
P3c1 (C^3_{3v})	6	1 (C_1)	$11A_1$		23E	

* 1R - infrared active; π - $\vec{E}\parallel c$; σ - $\vec{E}\perp c$; A - nondegenerate; E - doubly degenerate.

infrared or Raman studies. Only the $P\bar{3}c1$ lattice seems to be consistent with both infrared and Raman measurements.

The difference between the $P6_3/mcm$ and $P\bar{3}c1$ lattices is determined only by small displacements, however, which are of the same type as suggested by Oftedal, in 1931, to fully reconcile his x-ray measurements with his proposed structure.[12] The $P6_3/mcm$ lattice can be generated from the $P\bar{3}c1$ lattice by displacing the four "d" fluorines by 0.46 Å[16] so that they lie in horizontal mirror planes perpendicular to the c axis at $z = \pm \frac{1}{4}$ lattice units and by displacing the twelve "g" fluorines by 0.04 Å[16] so that they are contained within vertical mirror planes passing through the origin and the lanthanide ions. The net result of these displacements is that two B_{2u} infrared inactive modes and the four A_{2u} infrared active modes of the D_{6h} group combine to form the six A_{2u} infrared active modes of the D_{3d} group. Four inactive E_{2u} modes and the seven active

B_{1u} modes of D_{6h} combine to form the eleven E_u modes of D_{3d}. Therefore, the infrared spectrum associated with the $P\bar{3}c1$ lattice may be expected to consist of 4 (z) and 7 (xy) strong reflection bands, characteristics of the $P6_3/mcm$ lattice, together with two more (z) and four more (xy) weaker reflection bands allowed only in the $P\bar{3}c1$ lattice. The experimental results confirm this, and at 295°K the weaker bands observed at lower temperatures are almost completely damped out, leaving just 7 (xy) and 4 (z) infrared active modes. This result might also be expected because the small distances that differentiate between these two lattices are comparable with typical vibrational amplitudes of ions in solids, and the increased amplitude of these vibrations as the temperature is raised would more strongly affect the weaker bands allowed only in the $P\bar{3}c1$ lattice.

In addition to adequately explaining the optically active phonon spectrum, the $P\bar{3}c1$ lattice has a lanthanide ion site symmetry low enough to be compatible with all of the reported optical absorption measurements, and has fluorine ion sites compatible with the spectra of H^- and D^- impurities in the lattice.[23] Those experiments in which polarized or partially polarized electronic spectra have been observed do not necessarily contradict the low site symmetry found in the $P\bar{3}c1$ lattice, since the lower site symmetry merely allows unpolarized transitions, and the depolarization of a given transition need not easily be measurable.

6. Magnetic Space Group

In spite of our evidence supporting the $P\bar{3}c1$ lattice, it is not the proper tysonite structure because it predicts a magnetic ordering that is inconsistent with some of the paramagnetic and nuclear magnetic resonance experiments. Only 3 magnetically inequivalent lanthanide sites are predicted for the $P\bar{3}c1$ structure,[19] yet 6 magnetically inequivalent sites have been observed.[19, 20]

This difficulty can be resolved by considering the 1651 Shubnikov groups,[37] which include the 230 conventional space groups (Fedorov groups) as a subset. The Shubnikov groups can be generated from the Fedorov groups by assigning positive (+) or negative (-) signs (or colors black and white) to the points of space, and defining a sign (or color) inversion (anti-identity) operator associated with these signs (or colors).[38] The addition of this new operation generates 230 major (polar or single color) space groups that are identical with the Fedorov groups and contain only the new identity operator, 230 major (grey or neutral) space groups that contain both the identity and the anti-identity operator, and 1191 minor (mixed polarity or black-white) space groups that contain some complementary operators, but not the anti-identity operator. Associated with these space groups are the 32 conventional (polar or single color) crystal classes, 32 (grey) crystal classes containing the anti-identity operator, and 58 minor crystal classes containing some complementary operators, but not the anti-identity operator.[37-39]

For this particular application of the Shubnikov groups, the anti-identity operator defined above will be considered to be a magnetic inversion operator. A complementary operation will have the same effect as the conventional operation followed by a reversal of the local magnetic field (equivalently: followed by a reversal of the electronic or nuclear spin generated by the conventional operator).

Table X-4 lists significant properties of the six magnetic space groups associated with the conventional $P\bar{3}c1$ lattice space group. Since the magnetic inversion operator does not affect physical displacement vectors or electric field vectors, any of these magnetic space groups that has the same space lattice will have the same phonon spectrum and the same optical absorption spectrum to the extent that magnetic effects can be ignored. The group $P_c\bar{3}c1$ is based upon one of the 22 new, mixed polarity lattices[37,40] rather than one of the 14 polar Bravais lattices. Since this latter group does not have a proper magnetic representation for the atomic sites occupied in the tysonite space

Table X-4. Significant properties of the possible tysonite magnetic space groups (extracted partly from refs. 37-40).

Magnetic Space Group	Magnetic Crystal Class	Number of Magnetically Distinguishable Lanthanide Sites	Number of Independent Constants†		
			Pyromagnetism $H_i = a_i T$	Magneto-Electric Polarizability $H_i = a_{ij} E_j$	Piezomagnetism $H_i = C_{ijk}\sigma_{jk}$
$P\bar{3}c1$	$\bar{3}m$	3	0	0	2
$P\bar{3}c1'$	$\bar{3}m1'$	3	0	0	0
$P\bar{3}'c1$	$\bar{3}'m$	6	0	1	0
$P\bar{3}'c'1$	$\bar{3}'m'$	6	0	2	0
$P\bar{3}c'1$	$\bar{3}m'$	3	1	0	4
$P_c\bar{3}c1$	$\bar{3}m$	*	0	0	2

†H_i - magnetic field; a_i - pyromagnetic tensor; T - temperature; a_{ij} - magneto-electro polarizability; E_j - electric field; C_{ijk} - piezomagnetic tensor; σ_{jk} - stress tensor.

*See text. No proper magnetic representation for atomic sites occupied in tysonite lattice.

lattice, it will not be discussed further. The other five magnetic space groups have the same space lattice as the conventional $P\bar{3}c1$ space group, therefore, they are all consistent with both the infrared and Raman studies reported above.

On account of the C_3 operator of the $\bar{3}m$ (D_{3d}) group, there will be at least 3 magnetically distinguishable lanthanide sites. If there are only three such sites, however, the lanthanide sites must be equivalent in pairs. Therefore, it is sufficient to determine whether any one lanthanide site is equivalent to the sites generated from it by the spatial inversion operator.

The grey magnetic space group $P\bar{3}c1'$ represents a magnetically disordered or nonmagnetic crystal. Because of the existence of the magnetic inversion operator in this group, there are no local internal magnetic fields at any point within the crystal, and Kramers degeneracies are unsplit. Upon the application of an external magnetic field, any degenerate electronic states may be Zeeman split. Since the group includes the magnetic inversion operator, however, the same splitting at that site must result when the external magnetic field is reversed. Therefore, independently of the assumed spatial or magnetic parity of a magnetic tensor property associated with them, the lanthanide sites generated from each other by the spatial inversion operator must be magnetically indistinguishable.

The magnetic space groups $P\bar{3}c1$ and $P\bar{3}'c'1$ both have 3 ordinary C_2 operators perpendicular to the c or the z axis of the crystal. If $\hat{x}$ is defined as a unit vector parallel to a C_2 axis passing through a given lanthanide site and $u = z \times x$, it can be shown that an external field applied perpendicular to the x axis (that is, in the u-z plane) must

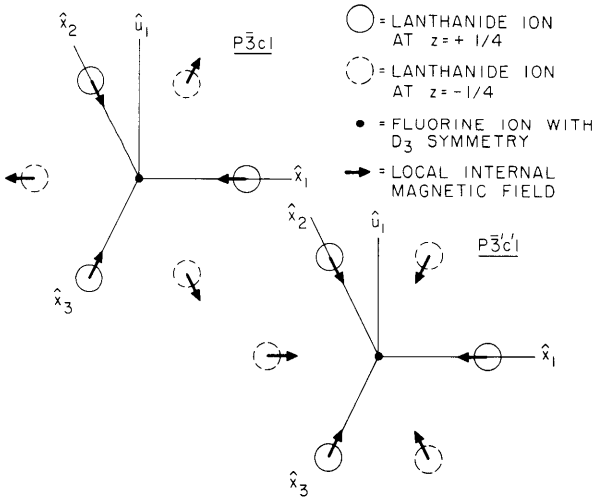

Fig. X-7. Local internal magnetic fields permitted at the lanthanide ion sites in the $P\bar{3}c1$ and $P\bar{3}'c'1$ structures.

generate the same splitting at that site, whether the field is positively or negatively directed. Therefore, just as for $P\bar{3}c1'$, the lanthanide sites generated from each other by the spatial inversion operator are indistinguishable by magnetic field established in their common u-z plane.

It may be possible, however, to distinguish these sites from one another by the x component of the external magnetic field. Figure X-7 shows the local magnetic field permitted at the lanthanide sites in these two structures. In the $P\bar{3}'c'1$ structure, the local internal magnetic fields at the two types of sites related by the spatial inversion operator are antiparallel. The external and internal magnetic fields add at one type of site and subtract at the other, thereby resulting in a different Zeeman splitting, and allowing the sites to be magnetically distinguished. In the $P\bar{3}c1$ structure, the local internal magnetic fields at these two types of sites are parallel. As a result, the total magnetic field and the resulting Zeeman splitting at both sites is the same, and the two types of sites are not magnetically distinguishable, even though the Zeeman splitting at a given site does change if the magnetic field is reversed.

By similar arguments it can be shown that $P\bar{3}c'1$ has only 3 magnetically distinguishable sites and is ferromagnetic, and $P\bar{3}'c1$ has 6 magnetically distinguishable sites and is antiferromagnetic. Since neither of these properties has yet been observed for the tysonite lanthanide fluorides, the only magnetic space group that simultaneously explains the optically active phonon spectra and the optical absorption spectra of ions in the lattice, and is consistent with the magnetic resonance data, is the $P\bar{3}'c'1$ magnetic space group.

As indicated in Table X-4, either $P\bar{3}'c'1$ or $P\bar{3}'c1$ can exhibit the magnetoelectric effect ($E_i = \sum_j a_{ij}H_j$, where $\vec{E} \equiv$ electric field, $\vec{H} \equiv$ magnetic field, and a_{ij} is the magnetoelectric tensor). $P\bar{3}'c1$ possesses only one off-diagonal antisymmetric tensor element, $a_{xy} = -a_{yx}$. $P\bar{3}'c'1$ has two diagonal symmetric tensor elements, $a_{xx} = a_{yy} \neq a_{zz}$. A study of the symmetry of this effect, if found in the tysonite lanthanide fluorides, could confirm the proposed $P\bar{3}'c'1$ magnetic structure.

7. Summary and Conclusion

Between 100 cm^{-1} and 500 cm^{-1}, the tysonite lanthanide fluorides LaF_3, CeF_3, PrF_3, and NdF_3 exhibit 5 or 6 infrared active (z) phonon modes when E // c and 10 or 11 infrared active (xy) phonon modes when E ⊥ c. These results, together with Raman results, are consistent with a $P\bar{3}c1$ space lattice, but not with any of the other space lattices proposed from x-ray diffraction studies.

Two additional strong infrared transitions at 66 cm^{-1} and 92 cm^{-1} are observed in PrF_3. These are attributable to electronic transitions from the ground state to the first and second excited states of the $^3H_4$ Stark multiplet of the Pr^{3+} ion. One additional

moderately strong infrared transition at 45 cm^{-1} is observed in NdF_3, because of an electronic transition from the ground state to the first excited state of the $^4I_{9/2}$ Stark multiplet of the Nd^{3+} ion.

Some of the reported magnetic resonance data are inconsistent with a $P\bar{3}c1$ magnetic space group, but all of the currently reported data on the tysonite lanthanide fluorides are consistent with a $P\bar{3}'c'1$ magnetic space group.

R. P. Lowndes, J. F. Parrish, C. H. Perry

References

1. S. A. Johnson, H. G. Freie, A. L. Schawlow, and W. M. Yen, J. Opt. Soc. Am. 57, 734 (1967).
2. R. A. Buchanan, H. E. Rast, and H. H. Caspers, J. Chem. Phys. 44, 4063 (1966).
3. W. F. Krupke and J. B. Gruber, J. Chem. Phys. 39, 1024 (1963).
4. E. V. Sayre and S. Freed, J. Chem. Phys. 23, 2066 (1955).
5. R. P. Bauman and S. P. S. Porto, Phys. Rev. 161, 842 (1967).
6. J. B. Mooney, Infrared Phys. 6, 153 (1966).
7. G. Hass, J. B. Ramsey, and R. Thun, J. Opt. Soc. Am. 49, 116 (1959).
8. Optovac Inc., North Brookfield, Massachusetts.
9. D. R. Bosomworth, Solid State Communs. (U.S.A.) 5, 681 (1967).
10. I. Oftedal, Z. Physik. Chem. 5B, 272 (1929).
11. I. Oftedal, Z. Physik. Chem. 13B, 190 (1931).
12. K. Schlyter, Arkiv Kemi 5, 73 (1953).
13. M. Mansmann, Z. anorgan. allgem. Chemie 331, 98 (1964).
14. M. Mansmann, Z. Kristallog. 122, 375 (1965).
15. A. Zalkin, D. H. Templeton, and T. E. Hopkins, Inorg. Chem. 5, 1466 (1966).
16. J. H. Van Vleck and M. H. Hebb, Phys. Rev. 46, 17 (1934).
17. J. Becquerel, W. J. de Haas, and J. Van den Handel, Physica 1, 383 (1934).
18. M. B. Schulz and C. D. Jeffries, Phys. Rev. 149, 270 (1966).
19. J. M. Baker and R. S. Rubins, Proc. Phys. Soc. (London) 78, 1353 (1961).
20. D. A. Jones, J. M. Baker, and D. F. D. Pope, Proc. Phys. Soc. (London) 74, 249 (1959).
21. A. Hadni and P. Strimer, Compt. Rend. 265, B811 (1967).
22. G. D. Jones and R. A. Satten, Phys. Rev. 147, 566 (1966).
23. H. H. Caspers, H. E. Rast, and R. A. Buchanan, J. Chem. Phys. 42, 3214 (1965).
24. H. H. Caspers, H. E. Rast, and R. A. Buchanan, J. Chem. Phys. 43, 2124 (1965).
25. W. M. Yen, W. C. Scott, and A. L. Schawlow, Phys. Rev. 136, A271 (1964).
26. A. Hadni, X. Gerbaux, G. Morlot, and P. Strimer, Japan. J. Appl. Phys. 4, 574 (1965); or see Proc. Conference on Photographic and Spectroscopic Optics (1964).
27. E. Y. Wong, O. M. Stafsudd, and D. R. Johnston, J. Chem. Phys. 39, 786 (1963).
28. E. Y. Wong, O. M. Stafsudd, D. R. Johnston, Phys. Rev. 131, 990 (1963).

29. H. H. Caspers, R. A. Buchanan, and H. R. Marlin, J. Chem. Phys. 41, 94 (1964).

30. H. E. Rast, H. H. Caspers, S. A. Miller, and R. A. Buchanan, Phys. Rev. 171, 1051 (1968).

31. C. H. Perry, R. Geick and E. F. Young, Appl. Opt. 5, 1171 (1966).

32. A. S. Barker, Jr., Ferroelectricity, edited by Edward F. Weller (Elsevier Publishing Company, Amsterdam, 1967), pp. 219-250.

33. D. W. Berreman and F. C. Unterwald, Phys. Rev. 174, 791 (1968).

34. J. F. Parrish, Ph.D. Thesis, Department of Physics, M.I.T., 1969.

35. A. Zalkin and D. H. Templeton, J. Am. Chem. Soc. 75, 2453 (1953).

36. International Tables for X-ray Crystallography, Vol. I (The Kynoch Press, Birmingham, England, 1965).

37. N. V. Belov, N. N. Neronova, and T. S. Swirnova, Soviet Phys. – Cryst. 2, 311 (1957).

38. A. M. Zamorzaev, Soviet Phys. – Cryst. 2, 10 (1957).

39. S. Bhagavantam and P. V. Pantulu, Proc. Indian Acad. Sci. 59, 1 (1964).

40. S. Bhagavantam and P. V. Pantulu, Proc. Indian Acad. Sci. 63, 391 (1966).

B. FAR INFRARED ELECTRONIC TRANSITIONS IN TYSONITE LANTHANIDE FLUORIDES

1. Introduction

The 4f electron shell of the lanthanide ions is so well shielded from its external environment that the effects of a crystalline electric field can usually be considered to be only a moderate perturbation of the free ion energy levels. Consequently, the 4f → 4f electronic transitions may be quite sharp within suitable crystals. As mentioned in Section X-A, it is possible that some of the 4f → 4f transitions, especially those between the Stark levels of a given multiplet, may be used to generate coherent far infrared radiation. The host lattice must be chosen with some care, however, as it will affect the lifetime of an electronic state, as well as the transition frequencies, strengths, and polarizations.

The tysonite lanthanide fluorides have a rugged structure[1,2] into which other lanthanide ions may be substituted up to at least one mole per cent.[3] Now that the symmetry of the lattice and the frequencies of the fundamental long wavelength ($k \approx 0$) infrared (see Sec. X-A) and Raman[4] active phonon transitions are known, the frequencies strengths, half-widths, and polarizations of the lowest frequency electronic transitions can be directly observed and unambiguously identified. Such observations can confirm the currently proposed assignments of the crystalline Stark levels of the electronic ground states, which previously have been based upon measurements made only in the near infrared, as well as yield otherwise inaccessible details of the symmetry and the

multipole strengths of the local electric field within the crystal.

The electronic transitions of Pr^{3+}, Nd^{3+}, Sm^{3+}, and Er^{3+} in LaF_3, which have been predicted to lie below the lowest frequency infrared active fundamental phonon transition near 100 cm^{-1}, are particularly well suited for such direct observation. Based upon both near infrared[5-8] and far infrared[9] measurements, two of the Pr^{3+} ion transitions may be visible below 100 cm^{-1}. The first is predicted to be at 56 cm^{-1} in LaF_3, and at 66 cm^{-1} in PrF_3. The second should be at 80 cm^{-1} in LaF_3, and 90 cm^{-1} in PrF_3. Near infrared measurements predict such transitions at 45 cm^{-1} for Nd^{3+} in LaF_3,[10-12] at 48 cm^{-1} for Sm^{3+} in LaF_3,[13] and at 52 cm^{-1} for Er^{3+} in LaF_3.[14] Reported here are direct polarized observations of these transitions of Pr^{3+}, Nd^{3+}, and Er^{3+} in the tysonite lattices of LaF_3, CeF_3, PrF_3, and NdF_3. The proposed 48 cm^{-1} transition of Sm^{3+} could not be observed in LaF_3. Indirect evidence suggests that the 48 cm^{-1} satellites observed in the near infrared may be due, in fact, to vibronic transitions involving an otherwise silent, fundamental $k \approx 0$ phonon near 50 cm^{-1}, rather than involving a Stark level of the electronic ground state.

2. Experiment

All of the transmittance measurements were taken on an R.I.I.C. FS-520 Fourier spectrometer, a far infrared Michelson interferometer, which has been adapted for 12-bit analog-to-digital conversion. A 125-W mercury arc source was used in conjunction with a liquid-helium-cooled quartz filter and Ga-doped germanium bolometer detector. A vacuum-evaporated one-dimensional wire grid polarizer was used to reduce the horizontally polarized radiation to much less than 1% of the vertically polarized component.

Single crystal rods of LaF_3, CeF_3, PrF_3, and NdF_3 doped with one mole per cent of appropriate lanthanide ions, and oriented with the c axis parallel to the 10-mm diameter face and perpendicular to the 5-mm long axis of the rod were obtained from Optovac Inc.[3] Depending upon the observed transition strengths, the dope samples were cut and polished to thicknesses between 0.7 mm and 1.7 mm. The transmittance of LaF_3 with 1% Sm^{3+} was observed in samples that were 2 mm to 5 mm thick. These oriented slices were placed in a high-purity copper block sample holder attached to a liquid-helium reservoir. The temperature of the copper block at a point below the sample aperture was measured with a calibrated semiconductor resistance thermometer to be constant within 0.1 °K for any single set of measurements between the limits of 5 °K and 8 °K

The normalized transmittance was calculated from a ratio of the observed spectral transmittance of the sample to that of an aperture of the same size as the sample. The absorption coefficient was calculated from the approximate formula

$T(\omega) \approx (1-R(\omega))^2 \exp(-OC(\omega)d)$, where $T(\omega)$ is the observed transmittance, $R(\omega)$ is the observed reflectance, $OC(\omega)$ is the absorption coefficient, and d is the average thickness of the sample.

3. Results

Figure X-8 shows the absorption coefficient of LaF_3 between 40 cm^{-1} and 150 cm^{-1} in both the $\pi(E \parallel c)$ and $\sigma(E \perp c)$ polarizations. The sharp narrow peak at 107.7 cm^{-1} in the π-polarization has been identified as absorption attributable to the lowest frequency longitudinal optical (LO) phonon mode of LaF_3. As explained in Section X-A, coupling to this mode is possible because the c axis of the crystals is not precisely parallel to the crystal face. Similar absorption peaks can be observed in CeF_3, PrF_3, and NdF_3, and are also attributed to phonon transitions, rather than electronic transitions. Likewise, many moderately strong absorption bands observed below 40 cm^{-1} can be attributed to multiphonon transitions, rather than electronic transitions, because they are observed with the same strength and in the same locations, independently of the 1% dopings of other lanthanide ions in a host lattice. Since these higher order phonon transitions have not yet been completely assigned, electronic and vibronic transitions in this region cannot be unambiguously identified, and possible Stark levels below 40 cm^{-1} will not be discussed further in this report.

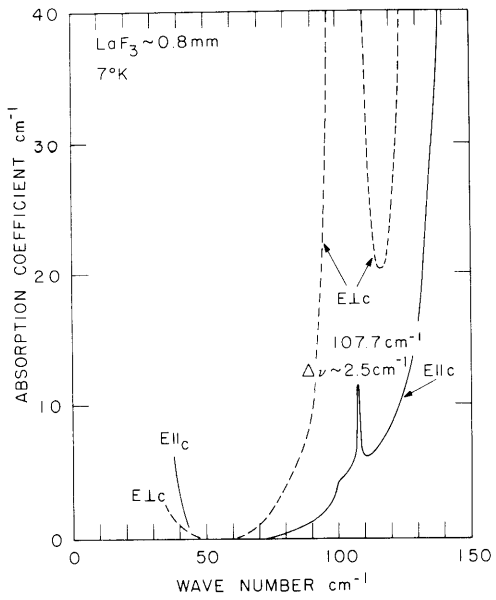

Fig. X-8.
Absorption coefficient of LaF_3 from 40 cm^{-1} to 150 cm^{-1}.

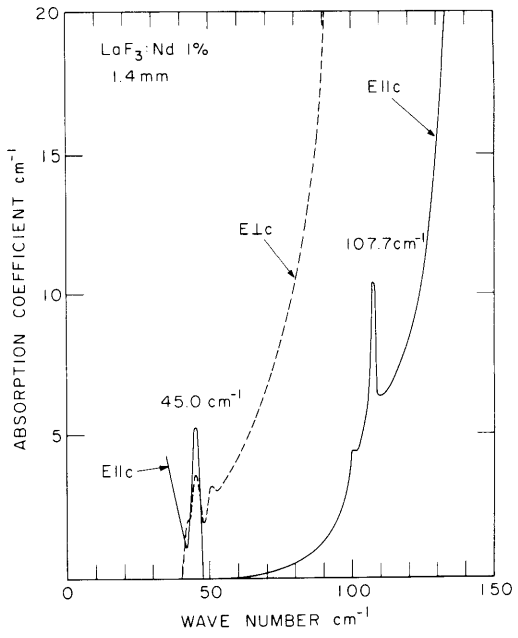

Fig. X-9.
Absorption coefficient of LaF_3:Nd 1% from 40 cm^{-1} to 150 cm^{-1}.

Figure X-9 shows the absorption coefficient of LaF_3 with 1% Nd^{3+}. Only one electronic transition, at 45 cm^{-1} in both polarizations, can be observed. The transition is slightly stronger in the π-polarization, but essentially it is unpolarized, in agreement with the predictions based upon a C_2 site symmetry in a $P\bar{3}'c'1$ structure (see Sec. X-A). Figure X-10 shows the Zeeman splitting observed in an unoriented slice of LaF_3 with 1% Nd^{3+} in fields up to 150 kG, which confirms the electronic nature of the 45 cm^{-1} Nd^{3+} transition.

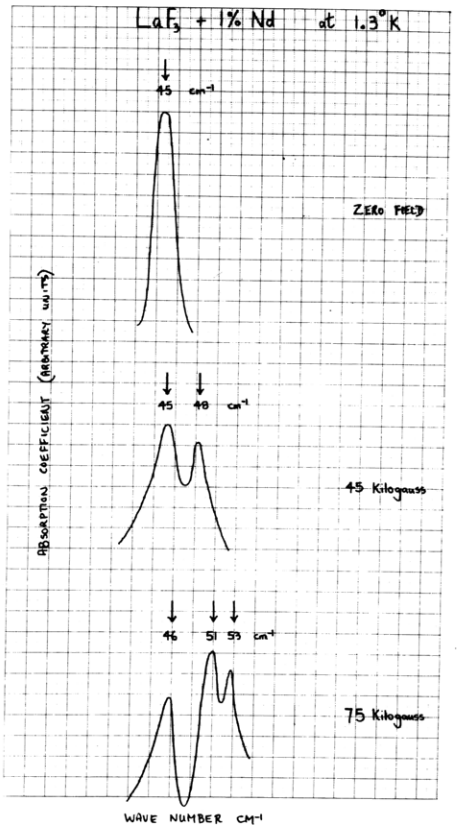

Fig. X-10.
Relative spectral absorption of LaF_3:Nd 1% in a magnetic field.

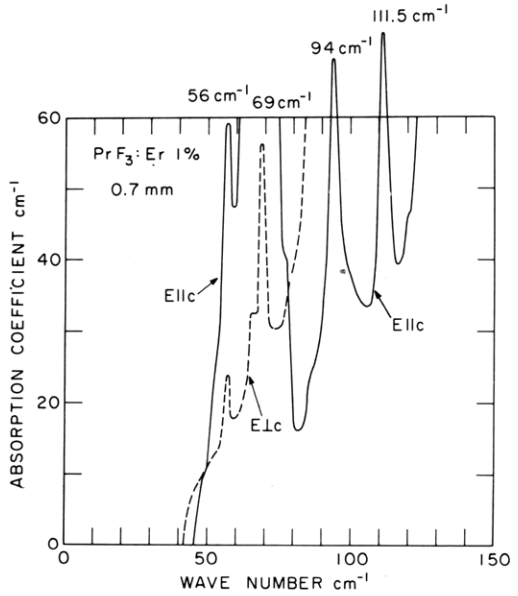

Fig. X-11.
Absorption coefficient of PrF_3:Er 1% from 40 cm^{-1} to 150 cm^{-1}.

Figure X-11 shows the absorption coefficient of PrF_3 with 1% Er^{3+}. The Er^{3+} transition at 56.8 cm^{-1} in PrF_3 is stronger in the π-polarization, yet the transition is unpolarized, as predicted. This Er^{3+} transition at 52 cm^{-1} in LaF_3 has also been Zeeman split, thereby confirming its electronic nature. The almost totally π-polarized 66 cm^{-1} transition of Pr^{3+} in PrF_3 is weakly observed at 66 cm^{-1} in the σ-polarization. The 69 cm^{-1} transition observed in the σ-polarization is probably related to the longitudinal

Table X-5. Electronic transitions below 100 cm^{-1} in tysonite lanthanide fluorides.

Ion \ Lattice		LaF_3		CeF_3		PrF_3		NdF_3	
		π	σ	π	σ	π	σ	π	σ
Pr^{3+} (I)	Frequency (cm^{-1})	56.5		61.7		66.4	66.5	68.7	
	Half-width (cm^{-1})	3.0	?	6.0	?	2.5	<5	3.5	?
	Strength (cm^{-2})	84		110		4000	<210	90	
Pr^{3+} (II)	Frequency (cm^{-1})		80.0				92.0		
	Half-width (cm^{-1})	?	4.5	?	?	?	2.0	?	?
	Strength (cm^{-2})		78				9000		
Nd^{3+}	Frequency (cm^{-1})	45.0	45.0	45.5	45.5	46.0	46.0		
	Half-width (cm^{-1})	3.0	3.0	4.0	4.0	4.0	4.0		
	Strength (cm^{-2})	19	13	27	20	10	12		
Er^{3+}	Frequency (cm^{-1})	52.0	52.0	53.5	53.5	56.8	56.8	57.7	57.7
	Half-width (cm^{-1})	4.0	4.0	3.5	3.5	4.0	4.0	4.0	4.0
	Strength (cm^{-2})	?	?	32	42	280	110	?	?

frequency of the electronic transition, but it cannot be adequately explained by a misalignment of the crystal axes, as can the 94 cm^{-1} and 111.5 cm^{-1} peaks in the absorption coefficient observed in the π-polarization.

Table X-5 lists polarized measurements of the frequencies, strengths, and half-widths of the electronic transitions of Pr^{3+}, Nd^{3+}, and Er^{3+} in LaF_3, CeF_3, PrF_3, and NdF_3.

All of the samples of LaF_3 with 1% Sm^{3+} up to 5 mm thick were essentially transparent between 40 cm^{-1} and 60 cm^{-1}. Thus, if the proposed 48 cm^{-1} level is truly electronic, its transition dipole strength must be much more than an order of magnitude weaker than those observed for Pr^{3+}, Nd^{3+}, and Er^{3+} transitions. The fact that several of the proposed multiplets of Sm^{3+} have a level 48-50 cm^{-1} above the lowest level and that the reported vibronic spectrum[15] of the $^3P_0$ level 20,926 cm^{-1} above the electronic ground state of 7% Pr^{3+} in LaF_3 also shows a level slightly below 50 cm^{-1} suggests that there may be an otherwise silent phonon mode near 50 cm^{-1}.

4. Present Research

The observed Stark levels of Pr^{3+}, Nd^{3+}, and Er^{3+} in LaF_3, CeF_3, PrF_3, and NdF_3 are now being compared with the frequencies, strengths, and polarizations theoretically predicted by the electric field that is expected at the lanthanide sites in the previously determined tysonite structure. Such an analysis should explain the almost total polarizations of the observed Pr^{3+} transitions, and, we trust, predict accurately the expected levels of the Sm^{3+} ion.

We wish to acknowledge the use of the facilities of the Francis Bitter National Magnet Laboratory, M.I.T., and to thank Richard W. Stimets for his cooperation and assistance in taking the transmission measurements at high magnetic field strengths.

J. F. Parrish, R. P. Lowndes, C. H. Perry

References

1. J. B. Mooney, Infrared Phys. 6, 153 (1966).
2. G. Hass, J. B. Ramsey, and R. Thun, J. Opt. Soc. Am. 49, 116 (1959).
3. Optovac Inc., North Brookfield, Massachusetts.
4. R. P. Bauman and S. P. S. Porto, Phys. Rev. 161, 842 (1967).
5. H. H. Caspers, H. E. Rast, and R. A. Buchanan, J. Chem. Phys. 43, 2124 (1965).
6. W. M. Yen, W. C. Scott, and A. L. Schawlow, Phys. Rev. 136, A271 (1964).
7. E. Y. Wong, O. M. Stafsudd, and D. R. Johnston, J. Chem. Phys. 39, 786 (1963).
8. E. V. Sayre and S. Freed, J. Chem. Phys. 23, 2066 (1955).
9. R. A. Buchanan and M. A. Butler, NAVWEPS Report 6852, p. 33.
10. S. A. Johnson, H. G. Freie, A. L. Schawlow, and W. M. Yen, J. Opt. Soc. Am. 57, 734 (1967).

11. H. H. Caspers, H. E. Rast, and R. A. Buchanan, J. Chem. Phys. 42, 3214 (1965).
12. E. Y. Wong, O. M. Stafsudd, D. R. Johnston, Phys. Rev. 131, 990 (1963).
13. H. E. Rast and H. H. Caspers, NOLC Report 672, p. 1, 1966.
14. W. F. Krupke and J. B. Gruber, J. Chem. Phys. 39, 1024 (1963).
15. R. A. Buchanan and H. H. Caspers, Solid State Spectroscopy, Naval Ordnance Laboratory Corona, p. 49.

C. OPTICAL PHONONS IN LEAD TITANATE

1. Introduction

$PbTiO_3$ is a ferroelectric at room temperature with a Curie temperature (T_c) of ~760 °K. Above T_c it exists as a cubic perovskite (space group O_h^1 Pm3m). Shirane et al.[1] have discussed this transition and have studied the dielectric properties in both phases.[2] The dielectric constant obeys the Curie-Weiss law above the transition temperature ($\epsilon \propto \frac{1}{T - T_c}$, where ϵ is the dielectric constant, and T the temperature), and suffers a very sharp decrease in value just below T_c. This transition is accompanied by a change in lattice symmetry to tetragonal (space group C_{4v}^1 P4mm) with lattice parameters a = 3.904 Å, c = 4.150 Å, c/a = 1.063.[3] This structure is isomorphous with tetragonal $BaTiO_3$, but does not display the further phase transitions seen in $BaTiO_3$. Another phase transition has been reported[4,5] at approximately 173 °K, apparently involving a change to a nonferroelectric form with a multiple unit cell, but it occurs only when the temperature is very slowly decreased. The further properties of this phase are not well known, at present. The substantial c/a ratio would indicate a much larger spontaneous polarization in $PbTiO_3$ than in $BaTiO_3$. Such drastic changes in the crystal structure are accompanied by large anomalies in the specific heat and volume.[2]

Perry et al.[6] have studied the infrared reflectance spectrum of $PbTiO_3$ ceramic at room temperature. This work extends these measurements to cover the temperature range 20-900 °K. Oriented crystals have been investigated in the infrared. Raman studies include both ceramics and single crystals over the same temperature range. The objectives of this research have been to assess the relative contributions of the various modes to the dielectric value below the Curie point and to determine their symmetries. An attempt is made to verify the existence of a multiple-unit-cell phase at lower temperatures.

The phonon mode symmetries and their participation in first- and second-order Raman and infrared interactions have been summarized in a previous progress report.[7] With the transition to tetragonal (C_{4v}) symmetry, all optical phonons of the cubic phase of F_{1u} symmetry become both infrared and Raman active (E and A_1). The F_{2u} mode

remains infrared inactive in only one of the three previously degenerate components (B_1), and all three become Raman active (B_1 and E). This permits a straightforward interpretation of the data as the Raman spectra should be primarily first-order (resulting from phonons at the center of the Brillouin zone).

2. Experiment

The $PbTiO_3$ samples used in this work were in both ceramic and single-crystal form. The ceramics were thin slabs ~0.5 mm thick, and roughly 1 cm square. The crystal samples were either small platelets or a large crystal embedded in epoxy with one face polished. All of the crystal types consisted of many small ferroelectric domains and only the epoxy-embedded sample contained regions of uniform domain orientation large enough to permit polarized studies in either the Raman or infrared regions. One region, ~2 mm square, contained the c axis nearly in the face of the crystal, and was oriented by using a polarizing microscope. Further examination revealed that while the region of uniform orientation was fairly large, the size of the domains was of the order of 0.1 mm. The differentiation between a and c axes was accomplished by means of Laue x-ray reflection. Study under the microscope also confirmed the general impression that the interior of the crystal was quite fragmented and in bad condition to perform experiments involving light in the visible region.

The low transmissivity of $PbTiO_3$ in the far infrared necessitated measurements of the wavelength-dependent reflectance. These experiments were performed in the 20-600 cm^{-1} region using a Michelson interferometer, and in the 250 cm^{-1}-1000 cm^{-1} region using a Perkin-Elmer Model 521 grating spectrometer. Resolution in both cases was approximately 5 cm^{-1}. Temperature control below 300°K was achieved with a cold-tail dewar, and control above room temperature with a nichrome heating element around a brass core embedded in Sauer-Eisen. These temperatures were measured using a copper-constantin thermocouple read with a transistorized null voltmeter. The higher temperature work was not performed on the epoxy-mounted sample, since (a) the epoxy would melt and/or decompose, and (b) cooling the sample after having subjected it to temperatures above T_c would almost certainly result in a new multi-domain structure, and very likely destroy the single area of good alignment that was found in the original sample. The extreme brittleness of $PbTiO_3$ also discouraged any attempt to obtain a small but good sample out of the larger crystal.

The Raman work was done on a Cary Model 81 spectrophotometer and, because of the physical configuration of the samples, utilized backscattered radiation from either a normally or obliquely incident He-Ne laser beam. Low temperatures were achieved using a Cryotip Joule-Thompson cycle refrigerator, and were measured using a Chromel-constantin thermocouple. High temperatures were produced by the sample holder used in the infrared measurements. Data were taken for all of the recorded

temperatures on the ceramic samples, but only at room temperature and lower on the epoxy-mounted crystal. Also, polarization studies were made on the latter, with the incident/scattered beams polarized/analyzed in all combinations of parallel or perpendicular to the c axis. The resolution used was normally 5 cm^{-1}, although some detailed studies were made at higher resolution.

3. Results

The infrared reflectance spectra from the two instruments were matched in the overlapping spectral regions by renormalizing the grating spectrometer data to the values given by the Fourier-transformed interferogram spectrum. These results were then subjected to a Kramers-Kronig (K-K) analysis[9] to derive the dielectric constant $\epsilon = \epsilon' + i\epsilon''$ and $\eta = \frac{1}{\epsilon} = \eta' + i\eta''$ from which were obtained the conductivity $\left(\sigma = \frac{\epsilon'' \nu}{2}\right)$ and the resistivity $\left(\rho = \frac{2\eta''}{\nu}\right)$, where ν is the frequency of the incident radiation. In Figs. X-12, X-13, and X-14 the room-temperature infrared results are presented for the two different types of sample and for the two different polarizations of the single-crystal studies. Below each of these figures is the result of the K-K analysis. In Fig. X-15 the low-frequency reflectance results may be seen at all temperatures for the ceramic sample. Each of these spectra is an average of at least two and of as many as six runs.

The Raman data are similarly an average of several retracings of the regions of interest, and spectra for several different temperatures may be seen in Fig. X-16. The gain change noted in the figure is due to the introduction of double-slit operation, which is feasible with the Cary 81 spectrophotometer above the 100 cm^{-1} to 200 cm^{-1} frequency shift. It is important to note that despite several attempts to find a dependence of these spectra on polarization, none was found in either the large oriented sample or the small platelets. There is no doubt that $PbTiO_3$ is tetragonal, which should lead to an exclusively diagonal Raman tensor for frequencies associated with an "A_1" symmetry phonon, and an exclusively nondiagonal one for the "E" modes. The orientations of the samples were quite well known, so the polarization of incident and scattered radiation could be selected parallel or perpendicular to the major crystallographic axes with some precision, and should have resulted in at least noticeable polarization effects. None were seen, however, and this suggests that the scattering volume in any variation of the Raman work involved a sufficiently large portion of the crystal to include the regions of severe defect noticed under optical examination. The frequencies of the various Raman lines and bands changed in a reproducible fashion with variations in temperature, but no qualitative change could be induced, either by slow cooling or by extreme heating with subsequent cooling to temperatures less than T_c. This was reassuring, since the material became a yellowish-orange

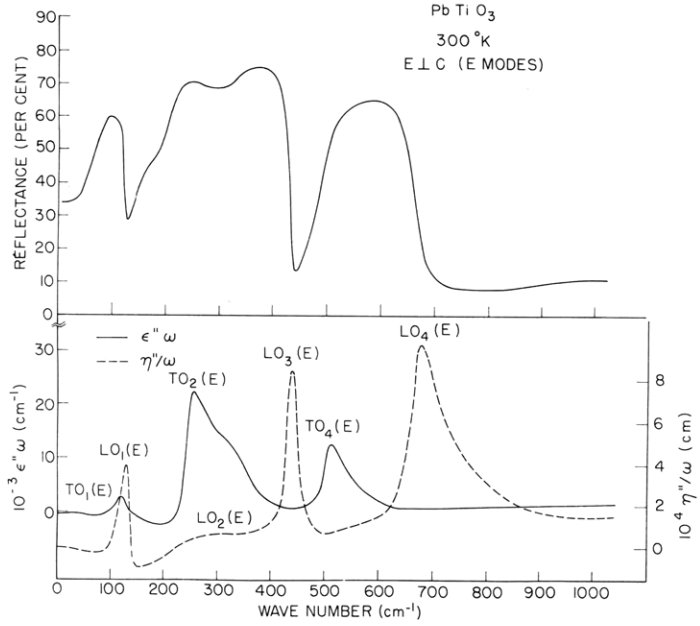

Fig. X-12. Infrared reflectance, conductivity, and resistivity of $PbTiO_3$ at room temperature. $\vec{E}$ polarized perpendicular to the c axis, thereby giving the E modes.

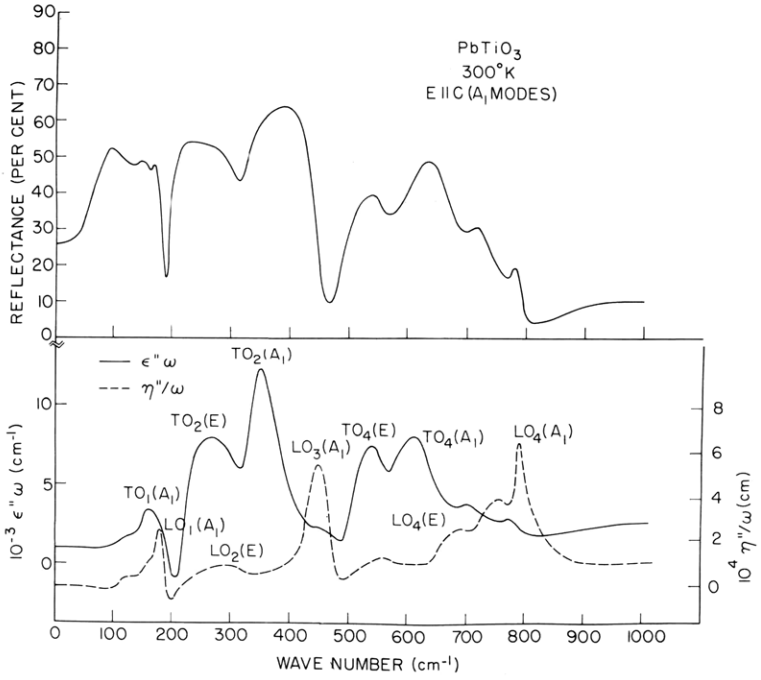

Fig. X-13. Infrared reflectance, conductivity, and resistivity of $PbTiO_3$ at room temperature. $\vec{E}$ polarized parallel to the c axis, thereby giving the A modes.

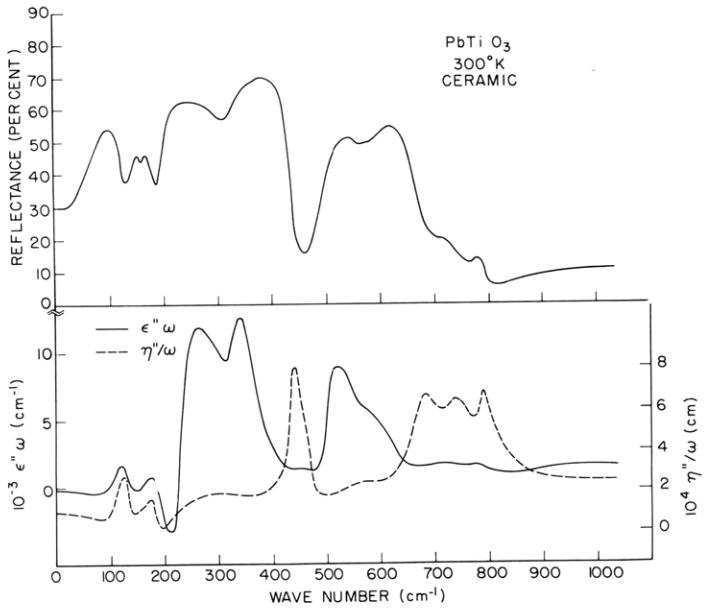

Fig. X-14.

Infrared reflectance, conductivity, and resistivity of $PbTiO_3$ ceramic at room temperature.

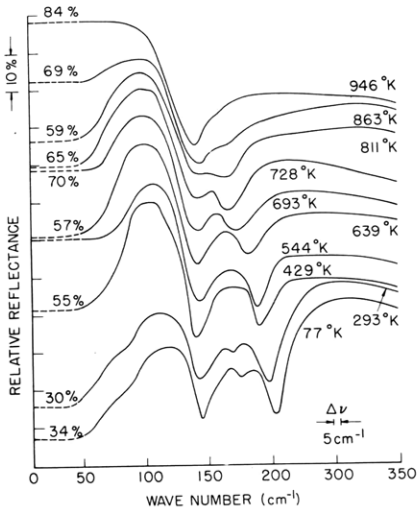

Fig. X-15.

Low frequency infrared reflectance spectra for ceramic $PbTiO_3$ at several temperatures.

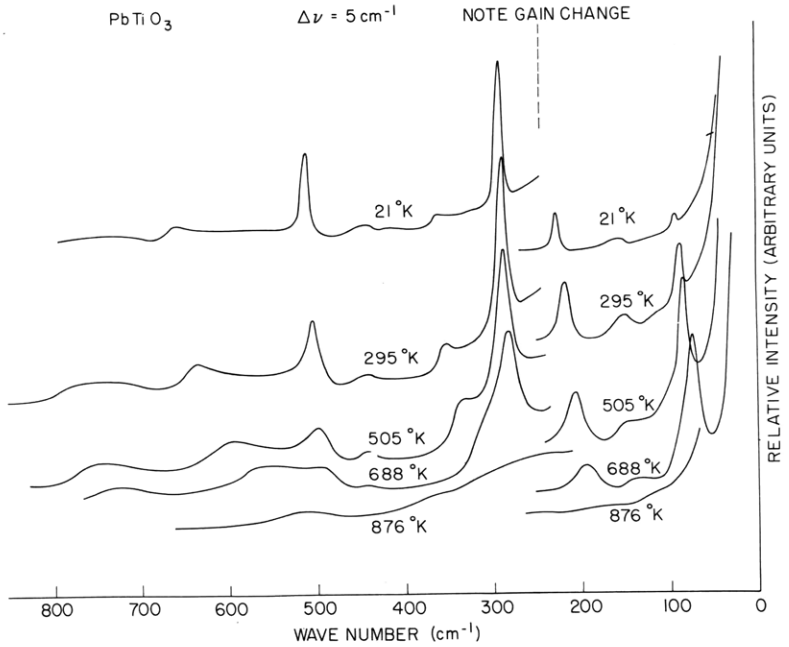

Fig. X-16. Raman spectra of $PbTiO_3$ at several temperatures.

above T_c, and there was some possibility that the sample had decomposed. The color change itself was reversible, however. Above T_c, the Raman spectra were exclusively second-order with very broad, indistinct structure. Finally, no difference could be seen between the spectra for oblique or orthogonal incidence. This could be expected, even if the phonon dispersion curves were substantially different for different directions in the crystal, since the relatively high refractive index for this substance results in a change of photon/phonon momentum transfer direction that is less than that required by the orientations of the pertinent wave vectors outside the crystal. Momentum is conserved by reflections at the surface of the material. Furthermore, the relatively large acceptance angle for the Raman equipment (roughly f/4) tends to include a large spread of momentum transfers for any scattering orientation, thereby leading to a large overlap in the phonon wave vectors observed between oblique and normal incidence. Finally, scattering from the defects discussed above would tend to complete the randomization of phonon wave vector direction observed. Of course, such considerations are irrelevant when discussing the results obtained from ceramic samples.

4. Discussion

The reluctance to use the epoxy-mounted sample at elevated temperatures necessitated the assumption that the ceramic behaved, spectroscopically, as the sum of results from all possible polarizations. From the infrared data presented in Figs. X-12, X-13, and X-14, this may seem to be the case at room temperature, and it was found to remain true at depressed temperature. Therefore the assumption seems valid.

The principal use of the infrared data is to distinguish first- from second-order Raman interactions. The frequencies of the transverse and corresponding longitudinal modes may be taken from those of the peaks in the conductivity and resistivity, respectively.[10] A comparison of the plots of these two quantities in each of Figs. X-12 through X-14 verifies that the splitting between the transverse and corresponding longitudinal mode is considerably less than that between transverse frequencies corresponding to the different phonon symmetries belonging to the same branch. This confirms the supposition, based on the large c/a ratio and specific heat and volume anomalies at T_c, that the anisotropy in the short-range forces is considerably greater than in the long-range electrostatic force.[11] The sharp distinction between the two polarizations indicates that the sample was reasonably well oriented, and is far superior to the Raman results principally because the high reflectivity prevents the electromagnetic field from experiencing the effects of the poorer regions of the crystal. The x-ray results were also well defined as a result of the relatively slight penetration of the crystal by the x-rays, because of its high lead content. It should be noted that the relatively higher complexity of the spectrum for $\vec{E}$ // c results from a slight

misorientation of the axes and a higher dielectric constant along the "a" axis than along the "c" axis of the crystal. The latter results in stronger coupling, with the radiation along this axis causing a small component of it lying in that direction to be affected relatively more strongly than the major component along the "c" axis. This causes a substantial superposition of "E" modes on a spectrum that should be principally from modes with "A_1" symmetry. The obverse is true for $\vec{E} \perp c$, thereby giving a very clean spectrum for the "E" modes. Note that the effect would be enhanced were the "c" axis not to lie exactly in the face of the crystal, a possibility not completely eliminated by the x-ray work, but minimized by the optical examinations.

In Fig. X-17 all of the infrared and Raman frequencies that were observed are plotted,

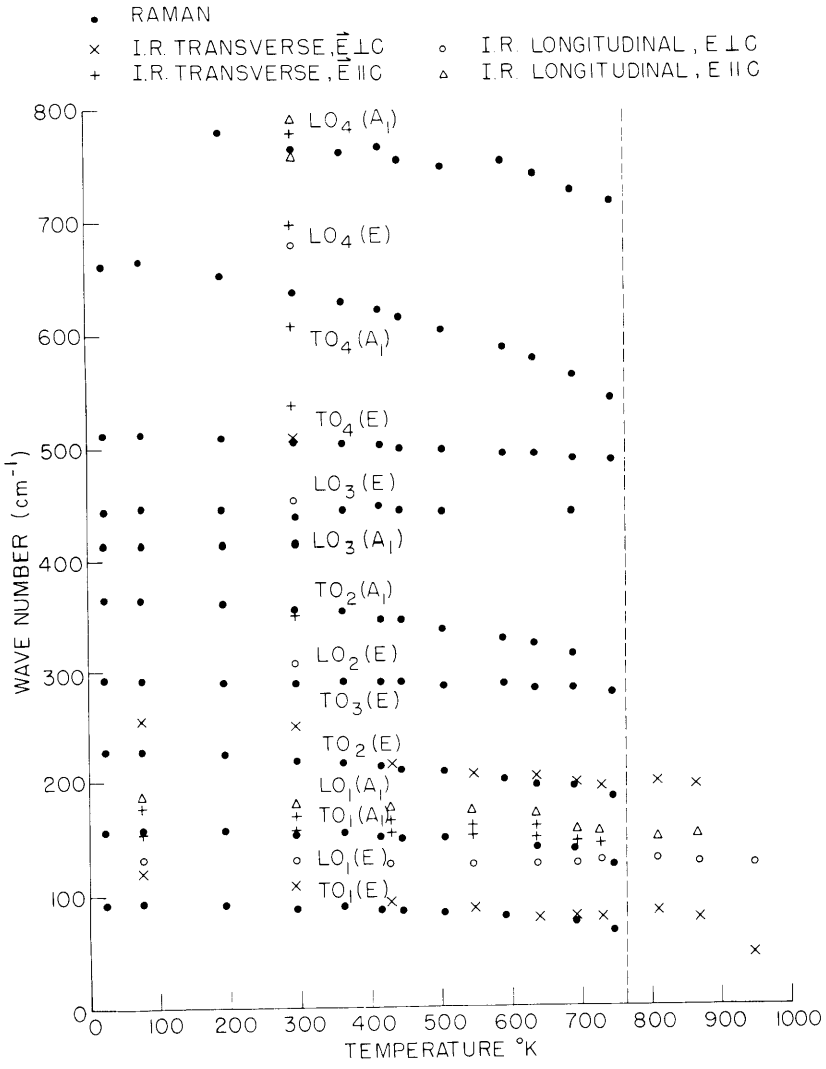

Fig. X-17. Raman and infrared frequencies vs temperature. Dotted line represents T_c.

together with their symmetry assignments. This allows the identification of the Raman spectrum as principally first-order. As can be seen, a majority of the lines are quite temperature-dependent. Figure X-18 shows the temperature dependence of the lowest

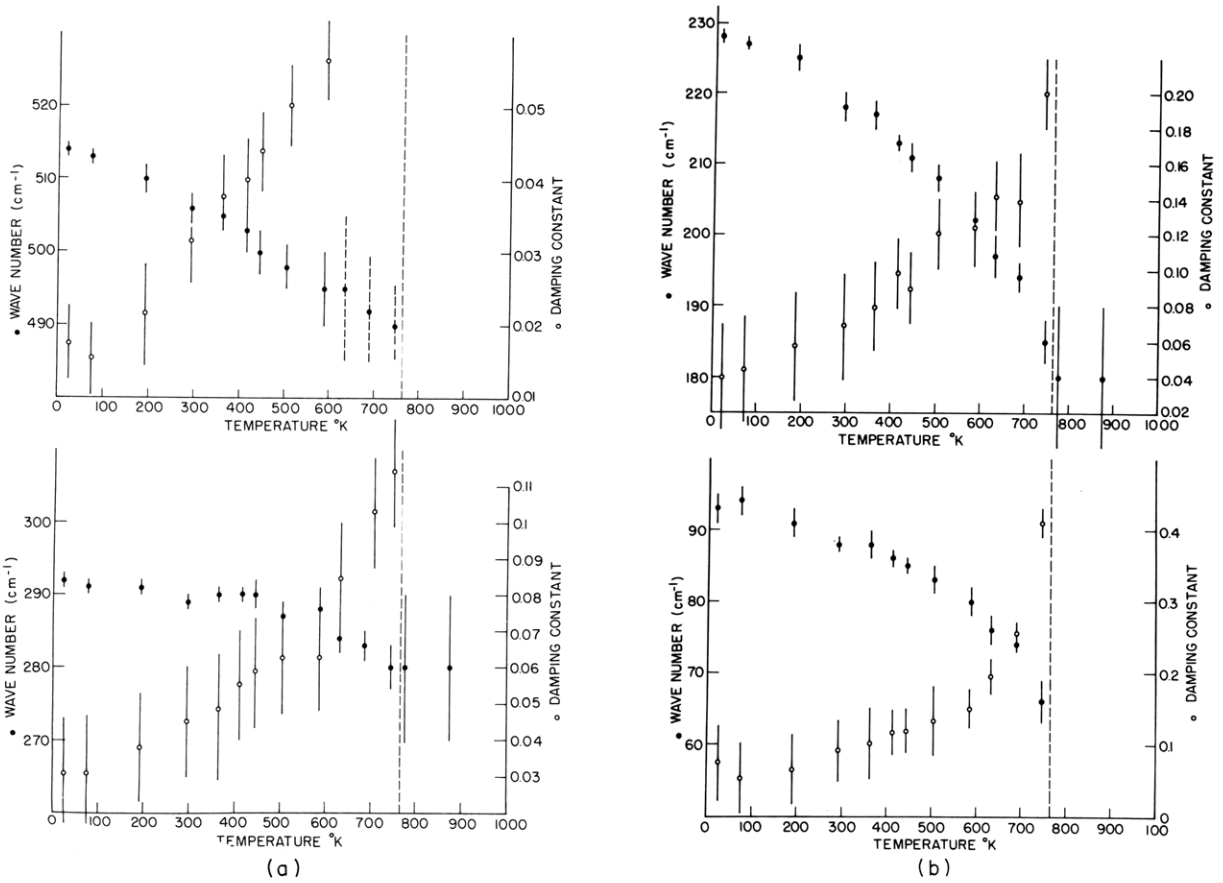

Fig. X-18. Temperature dependence of the E modes of $PbTiO_3$ and of their damping constant.

two transverse E modes and their corresponding damping constants. On the basis of the relationship[12, 13] $\epsilon \propto \frac{1}{\omega^2}$, such marked behavior would be expected to result in important contributions by many phonons to the dielectric constant below T_c. Barker[14] has written the Lyddane-Sachs-Teller relation for a multimode crystal with zero damping in differential form;

$$\frac{d\epsilon_o}{\epsilon_o} = \frac{2d\omega_{L_1}}{\omega_{L_1}} + \frac{2d\omega_{L_2}}{\omega_{L_2}} + \ldots - \frac{2d\omega_1}{\omega_1} - \frac{2d\omega_2}{\omega_2} \ldots,$$

where ω_j are the transverse phonon force parameters (related to the transverse phonon frequencies), ω_{L_j} are the longitudinal phonon frequencies, and ϵ_o is the static dielectric constant at the temperature under consideration. At room temperature $d\epsilon_o/\epsilon_o$ is approximately 0.002. The $TO_1(E)$ mode contributes ~0.0007 (~35%), the $TO_1(A_1)$ mode ~0.0003 (~15%), the $TO_2(E)$ mode ~0.0005 (~25%), and the $TO_4(E)$ mode ~0.0001 (~5%). As can be seen, the two lowest E modes account for approximately 60% of the observed value of $d\epsilon_o/\epsilon_o$. The equation above is strictly valid only for a particular vibration direction; however, ϵ_o was measured on a ceramic (whose ϵ_o may be lower than that of a single crystal) and the Raman data cover both polarizations. Consequently, only a rough check on the relative contributions of the modes can be made, and the total contribution may possibly be as high as 80%. The temperature dependence of the damping of the mode is also quite marked, and bears a striking resemblance to that found for $SrTiO_3$ by Fleury et al.[15]

Some of the lack of agreement between the Raman and infrared frequencies (Fig. X-16) could arise from the predominance of the anisotropic short-range forces already mentioned. If the crystal axes are not well aligned with the incident radiation, a phonon will be generated with the wave vector not along the major axes. This would give rise to a phonon that is neither longitudinal nor transverse, and whose frequency lies between those two extremes. This would result in a general broadening and shift of all first-order lines.

Because the Raman spectrum above T_c is exclusively second-order and quite indistinct, it cannot be used to study specific processes such as interactions with low-frequency phonons that would permit examination of soft-mode behavior. The infrared peaks, while representing first-order (zone center) interactions, are quite ill-defined and no consistent temperature dependence could be discerned within the temperature range that was attainable. Thus a study of soft-mode behavior in the paraelectric phase was not conducted.

Finally, although an apparent splitting may be noted in the low-frequency infrared data at lower temperatures, it can be seen to exist at room temperature. Furthermore, the lack of change in the Raman spectrum as the sample was cooled indicates that the size of the unit cell did not change, and thus the phase change proposed by Kobayashi[4,5] was not observed.

N. E. Tornberg, C. H. Perry

References

1. G. Shirane, S. Hoshino, and K. Suzuki, Phys. Rev. 80, 1105 (1950).
2. G. Shirane and S. Hoshino, J. Phys. Soc. Japan 6, 265 (1951).
3. H. D. Megaw, Proc. Phys. Soc. (London) 58, 10 (1946).
4. J. Kobayashi and R. Ueda, Phys. Rev. 99, 1900 (1955).

5. J. Kobayashi, S. Okamoto, and R. Ueda, Phys. Rev. 103, 830 (1956).

6. C. H. Perry, B. N. Khanna, and G. Rupprecht, Phys. Rev. 135, 408 (1964).

7. C. H. Perry, and N. E. Tornberg, Quarterly Progress Report No. 88, Research Laboratory of Electronics, M.I.T., Jaunuary 15, 1968, p. 41.

8. C. H. Perry and T. F. McNelly, Phys. Rev. 154, 456 (1967).

9. C. H. Perry, R. N. Khanna, and G. Rupprecht, Phys. Rev. 135, A408 (1964).

10. C. H. Perry and N. E. Tornberg (submitted for publication).

11. R. Loudon, Advances in Physics, Vol. 14, edited by N. F. Mott (Taylor and Francis, Ltd., London, 1964), p. 423.

12. W. Cochran, Advances in Physics, Vol. 9, edited by N. F. Mott (Taylor and Francis, Ltd., London, 1960), p. 387.

13. B. Szigeti, Trans. Faraday Soc. 45, 155 (1949).

14. A. S. Barker, Jr., in Ferroelectricity, edited by F. Weller (Elsevier Publishing Company, Amsterdam 1967), p. 238.

15. P. A. Fleury, J. F. Scott, and J. M. Worlock, Phys. Rev. Letters 21, 16 (1968).

D. LATTICE VIBRATIONS AND STRUCTURE OF AMMONIUM HALIDES

1. Introduction

The ammonium halides undergo a number of structural modifications under constant pressure at certain well-defined transition temperatures. These phase transformations have attracted considerable experimental and theoretical interest as there are associated discontinuities in several properties, such as the specific heat,[1,2] dielectric constant,[3] coefficient of expansion,[4] elastic constants,[5,6] lattice parameters,[7-9] and piezoelectric effects.[10] A generalized phase diagram showing the correlation among the phases has been given by Stevenson,[11] who claims that the only difference between the ammonium halides is the magnitude of the molecular volume.

The phase transformations and crystal structures in the ammonium halides are summarized in Table X-6.

The nature of these transitions has been studied in considerable detail in the near infrared by Hornig and his co-workers,[12-14] but the measurements have been restricted to the investigation of either the fundamental internal motions of the ammonium ion or combinations involving the lattice torsional or librational mode and the internal modes.

Neutron inelastic scattering measurements,[15-17] for the most part, have been concerned with the investigation of the librational mode, since this provides an experimental test of models of the order-disorder transformation. Complementary Raman measurements have been made on the ammonium halides by several workers,[18-21] and, in certain cases, these have included the study of the external lattice modes. In this report, further results[22,23] are presented of the vibrational states of the ammonium halides crystal lattices determined from both infrared and Raman spectroscopy and covering a wide temperature range. These studies include most of the various phase transformations, and the mode activities agree, in general, with the group theoretical predictions from the proposed structures in each phase.

Simple models of ionic solids lead to the Szigetti relations[24] that connect the infrared lattice reststrahlen frequency, the compressibility, the cell volume, and the dielectric constant. These relations may be subjected to experimental test and deviations from ideal behavior may lead to refinements in the models to allow for distortions and overlap of the electron-charge clouds.[25] Thus important modifications in the long-wavelength vibrational spectrum may be expected as the crystals undergo the different phase transitions. Unfortunately, only limited experimental data are available on the various parameters, especially in the low-temperature phases where these deviations can only be reliably evaluated and compared with the theoretical predictions.

Table X-6. Phase transformations in the ammonium halides.

Structure	Phase I (α) NaCl (disordered) O_h^5 (Fm 3m)	Phase II (β) CsCl (disordered) O_h^1 (Pm 3m)	Phase III (γ) (tetragonal) (antiparallel ordering) D_{4h}^7 (P4/nmm)	Phase IV (δ) CsCl (parallel ordering) T_d^1 (P4 3m)
NH_4Cl	α → 457.7°K	β	242.9°K	δ^* ←
ND_4Cl	α → 348.4°K	β	249.6°K	δ^* ←
NH_4Br	α → 411.2°K	β → 235°K	γ → 78°K 105°K	δ ←
ND_4Br	α → 405°K	β → 215°K	γ → 158°K 165°k	δ ←
NH_4I	α → 255.8°K	β → 231.8°K	γ	
ND_4I	α →	β →	γ	

*The ordered (δ) CsCl phase is generally referred to as Phase III in NH_4Cl and ND_4Cl.

2. Experimental Results

The spectroscopic investigations of the ammonium halides have been undertaken on thin sublimed films, crystalline powders, pressed pellets, and single crystals. The thin films were prepared by subliming the reagent grade salt onto polyethylene or crystal quartz substrates at room temperature. Films were approximately 1 μ, or less, thick, and appeared to be reasonably uniform. The crystalline powders were loosely packed in a hollow conical sample cell that was used in the Raman studies. The pressed pellets (~12 mm in diameter and 2 mm thick) were prepared by using a standard KBr press. Only single crystals of NH_4Cl and NH_4Br were available. The deuterated materials were prepared by repeated exchange, and the sublimed films were obtained in the same manner as the normal salts. The temperature-dependent studies were made by attaching the samples (or substrates) to a cold finger in a variety of cryostats. Low temperatures were obtained by using cryogenic refrigerants or a precooled gas-flow system. For detailed studies of the various phase transitions below room temperature, an Air-Products cryo-tip refrigeration system was used, which allowed temperatures to be attained in the range 300-20°K, with a temperature stability of ~±0.5°K. Temperatures were measured by thermocouples attached either to the samples or to the substrates. A calibrated germanium resistance thermometer was used in the liquid-helium temperature range.

High-temperature measurements in the Phase I modification of NH_4Cl and NH_4Br

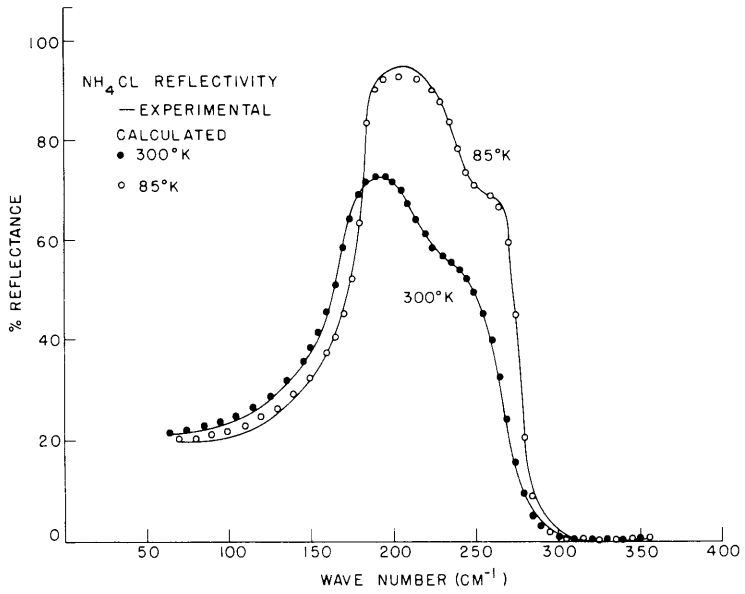

Fig. X-19. Reflectivity of single crystal NH_4Cl below and above the order-disorder phase transition.

were not reproducible because the materials readily sublimed in the vacuum of the instrument.

The infrared transmittance and reflectance measurements were performed on a Fourier-transform spectrometer with the aid of a low-temperature germanium detector.[26]

The Raman spectra were recorded on a Cary Model 81 spectrophotometer, with both the "Toronto" arc, mercury "e" line (4358 Å) and a Spectra-Physics 125 He-Ne laser (6328 Å) used as sources. Right-angle, oblique-angle, and backscattering geometries were used, depending on the type of sample and the excitation source. The intensities of the Raman bands and the background scattering depended on the sample (powder, pellet, or single crystal), and to some extent on the scattering geometry. The frequencies of the lines at a particular temperature were essentially independent of these effects. The NH_4Br single crystal could easily be supercooled to helium temperatures in the Phase III modification, and Phase IV could be completely obtained only by thermal cycling many times up to approximately 77°K. The pellet and powder, on the other hand, readily transformed into Phase IV, and hardly any thermal cycling was necessary. Similar effects were noticed with the NH_4I pellet, and occasionally it was difficult to obtain the tetragonal phase. Similar effects were noted in the x-ray investigations.[8]

For most phases the Raman tensor elements appeared to be mainly diagonal, but in

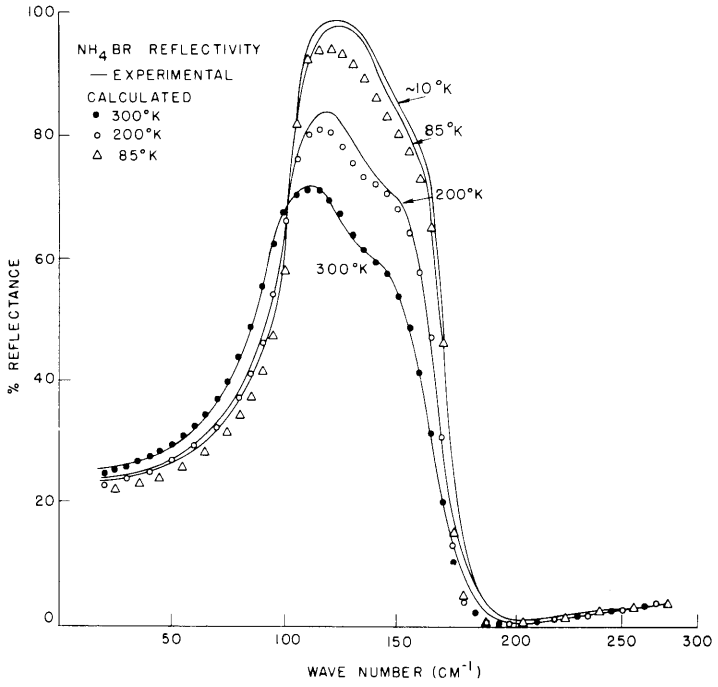

Fig. X-20. Reflectivity of single crystal NH_4Br in phases II, III, and IV.

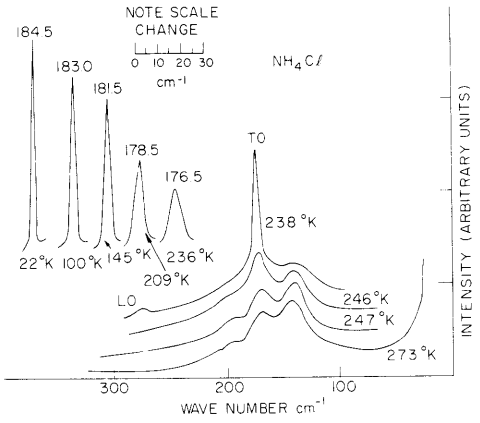

Fig. X-21. Raman spectra of NH_4Cl single crystal as a function of temperature.

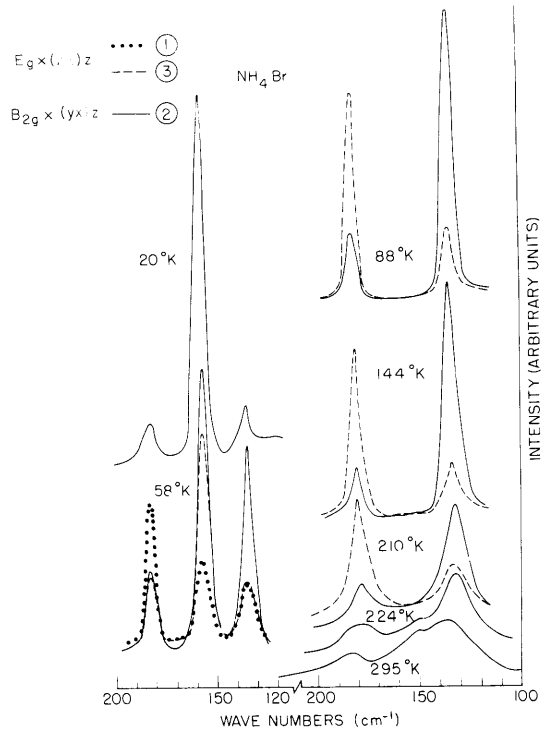

Fig. X-22. Raman spectra for NH_4Br single crystal as a function of temperature.

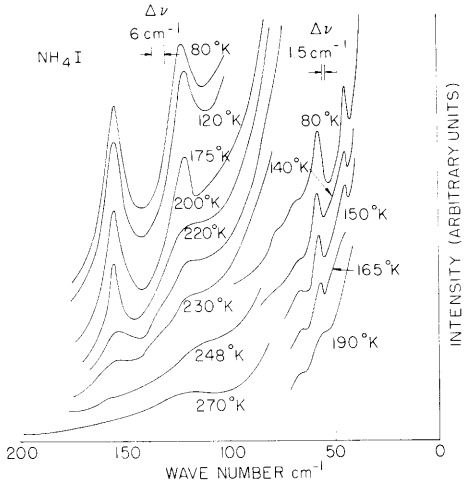

Fig. X-23. Raman spectra of NH_4I pressed disk (oblique angle scattering) as a function of temperature.

tetragonal NH_4Br it was possible to distinguish experimentally between the Raman tensor elements $\alpha_{xy} = \alpha_{yx}$ for $B_{2g}(\nu_5'')$ and $\alpha_{zy} = \alpha_{yz} = \alpha_{xz} = \alpha_{zx}$ for E_g (ν_5' and ν_7') phonons, and the results were consistent with the observation that the ν_6 (librational mode) also had E_g symmetry. This differentiation was not possible in NH_4I because a single crystal was not available.

The temperature-dependent infrared reflection measurements of single crystal NH_4Cl and NH_4Br are shown in Figs. X-19 and X-20. Portions of the low-frequency Raman spectra NH_4Cl, NH_4Br and NH_4I as a function of temperature are shown in Figs. X-21, X-22, and X-23, respectively.

3. Discussion

a. Group Theoretical Considerations

The crystal structure of the ammonium halides in the disordered states is NaCl (Phase I) and CsCl (Phase II) with "one" molecule per unit cell. The site mode symmetry for both the halide ion and the ammonium ion (as this is completely disordered) is O_h, and the only allowed external modes are two F_{1u} modes (one of which for $\underline{k} \approx 0$ is an infrared active translational mode (reststrahlen mode), and the other is an acoustic mode with $\nu = 0$) and an F_{1g} infrared and Raman silent librational mode.

In the ordered (parallel) cubic phase, with one molecule per unit cell, the structure is still CsCl, but the site mode symmetry of the ammonium ion is now T_d, whereas the halide ion remains O_h. The F_2 mode is now simultaneously infrared and Raman active.

The crystal structure in the tetragonal (antiparallel) phase has two molecules/unit cell, and belongs to the space group D_{4h}^7 (P4/nmm). The site symmetry of the ammonium ions is now D_{2d}, and that of the halide (only Br and I possess this phase) is C_{4v}.

The group theory of Halford and Hornig[27] predicts the following external lattice modes for the tetragonal modification.

$$(\text{External}) = A_{1g} + A_{2g} + B_{2g} + 3E_g + 2A_{2u} + B_{2u} + 3E_u$$

of which

$$(\text{Acoustic}) = A_{2u} + E_u$$

$$(\text{Translations}) = B_{2g} + E_g + A_{1g} + E_g + A_{2u} + E_u$$

$$(\text{Librations}) = A_{2g} + E_g + B_{2u} + E_u.$$

The correlations between the external lattice modes of the ammonium halide through the various phase transitions are shown in Table X-7. Also given are the activities and polarizations of the modes.

Table X-7. Correlation of the external lattice modes of NH_4Br through the various phase transitions.

	Molecular Modes Symmetry O_h (Phase I and Phase II)	Molecular Modes Symmetry T_d (Phase IV)	Site Modes Symmetry D_{2d}	Unit Cell Modes Symmetry D_{4h} (Phase III)
Translational Mode (ν_5)	F_{1u}(IR,–) (reststrahlen)	F_2(IR, R) (reststrahlen)	E(IR, R)	E_g(R) ν_5' (α_{zy}, α_{yz}, α_{xz}, α_{zx}) in phase
				E_u(IR) ν_5 out of phase (E ⊥ c) (reststrahlen)
			B_2(IR, R)	B_{2g}(R) ν_5'' (α_{xy}, α_{yx}) in phase
				A_{2u}(IR) ν_5 out of phase (E ∥ c) (reststrahlen)
Librational Modes (ν_6)	F_{1g}(–)	F_1(–)	E(IR, R)	E_g(R) ν_6' (α_{zy}, α_{yz}, α_{xz}, α_{zx})
				E_u(IR) ν_6 out of phase (E ⊥ c)
			A_2(–)	A_{2g}(–) in phase
				B_{2u}(–) out of phase
'Acoustical' Modes (ν_7)	F_{1u}(–) (zero root)	F_2(–) (zero root)	E(–, R)	E_g(R) ν_7' (α_{zy}, α_{yz}, α_{xz}, α_{zx}) in phase
				E_u(–) zero root-pure translation
			B_2(–, R)	A_{1g}(R) ν_7'' ($\alpha_{xx}+\alpha_{yy}$, α_{zz}) in phase
				A_{2u}(–) zero root-pure translation

b. Infrared Active Phonon Modes

The reflectivity measurements[22] on single-crystal NH_4Cl at 300°K (β phase) and 85°K (δ phase) (shown in Fig. X-19), and NH_4Br at 300°K (β phase), 200°K and 85°K (γ phase) and 10°K (δ phase) (shown in Fig. X-20) were subjected to a Kramers-Kronig analysis to obtain the TO and LO phonon frequencies from the dielectric function. The data were also fitted with a classical dispersion formula.

$$\epsilon(\nu) = \epsilon' - i\epsilon'' = \epsilon_\infty + \frac{S_T^2}{\nu^2 - \nu_T^2 - i\nu\gamma_T} + \frac{S_l^2}{\nu^2 - \nu_l^2 - i\nu\gamma_l},$$

where ϵ_∞ is the value of the dielectric constant at frequencies considerably higher than the dispersion frequency, ν_T. ν_l is a small additional oscillator needed to fit the reflectivity on the high-frequency edge. This sideband is probably due to a multiphonon process (such as TO(X) + TA(X), where X refers to the "X" point in the Brillouin zone). S_T and S_l and γ_T and γ_l are the associated oscillator strengths and damping constants, respectively. The latter are introduced in an ad hoc way to account for anharmonic effects. The parameters used in the classical oscillator model at the various temperatures are shown in Table X-8.

The thin-film transmission measurements are not shown, because of the large amount of data accumulated. The frequencies of the transverse modes may be seen graphically in Figs. X-24 through X-27 as a function of temperature for the three ammonium halides. The ND_4Cl and ND_4Br transmission spectra[23] are essentially similar to the normal salts, and the frequency shift is almost completely accounted for (within ~2%) by the increase in mass of the ammonium ion. According to Table X-7, the tetragonal phase in NH_4Br and NH_4I should yield two phonon modes corresponding to the E_u and A_{2u} species. It would appear from our results, however, that the frequencies are degenerate within experimental error. The spectral slit width in the infrared measurements was 3-4 cm^{-1}, and was dictated by the interferogram function. Any further increase in resolution (by simply increasing the maximum path difference in the interferometer) would not have changed the line shape of the transmission minimum. Consequently, it can only be assumed that in the case of NH_4Br the splitting is less than 4 cm^{-1}.

Durig and Antion[28] have found two infrared active bands in the tetragonal phase in NH_4I which may correspond to the E_u and A_{2u} vibrations, whereas our results indicate a degenerate mode as found in the bromide. Vedder and Hornig[14] state that a small amount of water vapor present in the NH_4I film in the NaCl phase, or their KBr substrate with an NaCl structure, was possibly responsible for the fact that this phase supercooled to liquid-helium temperatures. The former effect may be present in our NH_4I results during

Table X-8. Parameters used in the classical oscillator model to fit the infrared reflectivity of NH_4Cl and NH_4Br single crystals at various temperatures.

$$\epsilon(\nu) = \epsilon_\infty + \frac{s_1^2}{\nu^2 - \nu_T^2 - i\nu\gamma_T} + \frac{s_2^2}{\nu^2 - \nu_1^2 - i\nu\gamma_1}$$

	NH_4Cl		NH_4Br		
	300°K	85°K	300°K	200°K	85°K
s_T cm^{-1}	339.0	341.0	295.0	285.0	280.0
ω_T cm^{-1}	173.0	184.0	144.0	151.0	155.0
γ_T cm^{-1}	18.0	4.0	17.0	9.0	2.5
$\Gamma_T = (\gamma/\omega)_T$	0.10	0.02	0.12	0.06	0.02
s_1 cm^{-1}	87.0	52.0	52.0	55.0	48.0
ω_1 cm^{-1}	225.0	246.0	184.0	182.0	192.0
γ_1 cm^{-1}	45.0	32.0	30.0	28.0	38.0
ϵ_o	7.0	(6.0)	6.8	5.8	(5.2)
ϵ_∞	2.7	(2.7)	2.9	(2.9)	(2.9)
ω_ℓ cm^{-1}	273	281	224	226	229
$\omega_{\ell_{LST}}$ cm^{-1}	275	(275)	224	(216)	(213)

the transfer of the sample to the cryostat. This could explain why only one band is observed in our measurements. The reduced damping constant, $\Gamma = \gamma_T/\omega_T$ shows, however, a marked discontinuity at the 256°K phase transition. There was some evidence in our results that the frequency and shape of the band in NH_4I did depend to some extent on the substrate, but this effect needs to be investigated further.

One infrared active mode is observed in the disordered phases, and only one band is normally observed in the ordered (δ) or tetragonal (γ) phases, with an almost complete continuity through the phase transitions. The volume change is considerably less than 1% in all of the halides,[7,8] except in the Phase I to Phase II

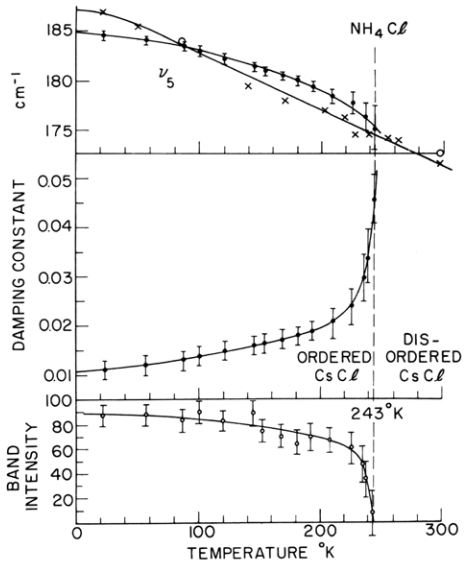

Fig. X-24.

Variation ν_5 in NH_4Cl determined from IR (X, thin film; O, reflectivity) and Raman (•) measurements. Plot of the Raman damping constant and band intensity as a function of temperature.

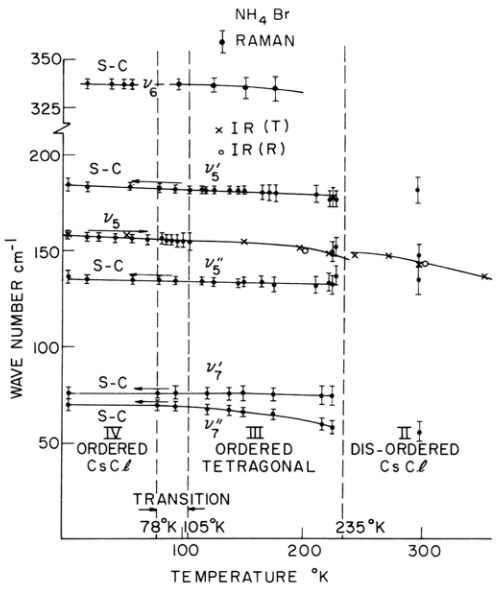

Fig. X-25.

Frequency variation of the IR and Raman modes through phases II, III, and IV in NH_4Br.

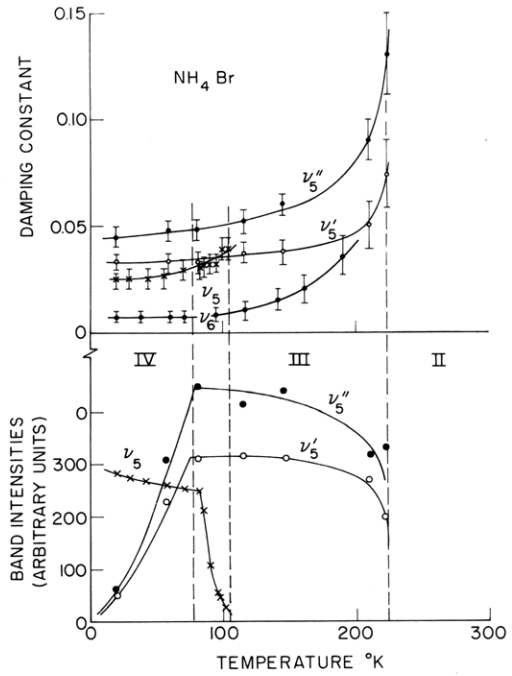

Fig. X-26.

Variation of the damping constants and band intensities for the Raman modes investigated as a function of temperature in NH_4Br.

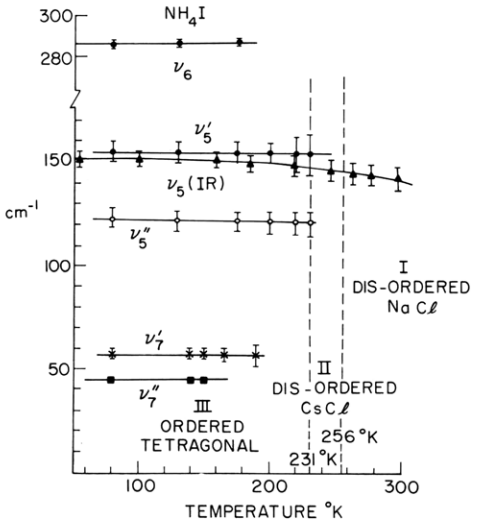

Fig. X-27.

Variation of the IR and Raman active lattice modes as a function of temperature in NH_4I. ν_5,Δ may possibly be in NaCl disordered phase I at all temperatures.

transition. The largest change occurs in the dielectric constant,[3] and it is this function that largely determines the temperature dependence of the modes.

The damping function, Γ, at low temperatures (~4°K) approaches ~0.02 in NH_4Cl, 0.025 in NH_4Br, and 0.15 in NH_4I. The temperature dependence is similar to that found in the alkali halides, namely 0.02 in RbCl, 0.014 in RbBr, 0.023 in NaBr, and 0.15 in LiI. The Γ's determined from the infrared reflectance measurements agree within 50% of those obtained from the Raman measurements where the mode is active in both. The transmission data yield Γ's roughly two to three times larger at low temperatures, whereas the room-temperature results agree within 20%. This is probably caused by imperfections in the thin films, because of strain, impurities, etc.; possibly, it is the major cause of the discrepancies in the frequency dependence with temperature in NH_4Cl (see Fig. X-24). The Raman Γ's are probably the most reliable, as they have been determined from the bulk single crystals.

c. Raman Active Phonon Modes

There should be no first-order allowed Raman bands in either the NaCl or CsCl disordered phases. All three materials exhibit moderately strong spectra, however, even at room temperature, and bands are observed at 140, 170, and 196 cm^{-1} in NH_4Cl, at 55, 135, and 185 in NH_4Br, and at 125 cm^{-1} in NH_4I. Tables X-9, X-10, and X-11 give a complete listing of all of the infrared and Raman modes seen in the ammonium halides, together with interpretations, and comparison can be made with the results obtained by other research workers. The modes listed above show similarity in some cases to the first-order Raman active modes observed in the ordered phases, and may be the remains of ordering of the ammonium ion, even though the crystal is strictly in a disordered phase. Alternatively, the spectrum could be predominantly second-order, and reflects a combined density of states spectrum derived from critical points at the Brillouin zone boundary. Possibly, it is some combination of both effects. In the tetragonal phase in NH_4Br, ND_4Br, and NH_4I all of the Raman active translational lattice modes are observed, and also the ν_6 librational mode.

The temperature-dependent damping constants of the Raman active modes in NH_4Br are plotted in Fig. X-26, together with the band intensities of ν_5, ν_5', and ν_5'', showing how they vary through the tetragonal to ordered cubic phase transition.

Loudon[29] has extended the theory of Raman scattering to cover piezoelectric crystals in which the mode is simultaneously infrared and Raman active (ordered NH_4Cl and NH_4Br). More first-order peaks should be observed due to a lifting of the group-theoretical degeneracy of polar lattice vibrations by long-range electrostatic forces that give rise to an additional electron-lattice interaction. In a cubic crystal both the phonon displacement and the electric field point in the same direction, so that the

Table X-9. Infrared and Raman frequencies of NH_4Cl and ND_4Cl in cm^{-1}.

		Thin Film Transmission	Reflectivity Kramers-Kronig	Reflectivity Dispersion		Raman	Others
NH_4Cl		ω_t	ω_t	ω_t	ω_ℓ		
(Phase II) 300°K	$(\nu_5)(F_{1u})$	172 ± 1	175 ± 2	173 ± 2 (225)	273 ± 5	(140) (170) (195)	155 neutron[17]
NH_4Cl							
(Phase III) 80°K	$(\nu_5)(F_2)$	185 ± 1	188 ± 2	184 ± 2 (246)	281 ± 5	188 ± 2 crystal[23] 188 ± 2 powder[22] (275 ± 5)	185 ± 6 neutron[15] 183 Raman[19]
ND_4Cl							
(Phase II) 300°K	$(\nu_5)(F_{1u})$	166 ± 2					
ND_4Cl							
(Phase III) 80°K	$(\nu_5)(F_2)$	177 ± 1				177 ± 2	

Frequencies in parentheses were all obtained from broad, weak bands and may be multiphonon in origin, or possibly indicate some small type of ordering found only in the tetragonal phase of NH_4Br and NH_4I.

Table X-10. Infrared and Raman frequencies of NH_4Br and ND_4Br in cm^{-1}.

		Thin Film Transmission	Reflectivity Kramers-Kronig	Reflectivity Dispersion		Raman	Others	
NH_4Br		ω_t	ω_t	ω_t	ω_ℓ			
(Phase II) 300°K	$(\nu_5)(F_{1u})$	147 ± 1	147 ± 2	144 ± 2 (184)	224	(185)(ν_5'?) (135)(ν_5''?)	148 ± 6 neutron[16]	160[17]
NH_4Br (Phase III) 200°K	$(\nu_5)(E_u, A_{2u})$	153 ± 2	154 ± 2	151 ± 2 (182)	226	(55)(ν_7?)		
	$(\nu_5')(E_g)$					179 ± 2	182	180[17]
	$(\nu_5'')(B_{2g})$					133 ± 2	136 Raman[19]	
	$(\nu_7')(E_g)$					75 ± 2	77	
	$(\nu_7'')(A_{1g})$					62 ± 2	69	
	$(\nu_6')(E_g)$					(330 ± 5)	335	
							333 neutron[17]	
NH_4Br (Phase IV) 20°K	$\nu_5(F_2)$	159 ± 2	159 ± 2	157 ± 2 (193)	229	157 ± 2 (225 ± 5)	165 ± 6[17] neutron 160[13] inferred	
ND_4Br (Phase II) 300°K	$\nu_5(F_{1u})$	138 ± 1						
ND_4Br (Phase III) 200°K	$\nu_5(E_u, A_{2u})$							
	$\nu_5'(E_g)$					165 ± 2		
	$\nu_5''(B_{2g})$					122 ± 2		
	$\nu_7'(E_g)$					75 ± 3		
	$\nu_7'(A_{1g})$					65 ± 3		
ND_4Br (Phase IV) 80°K	$\nu_5(F_2)$	147 ± 2				149 ± 2		

Frequencies in parentheses are all broad and weak. They may be multiphonon in origin, or may be the remains of some Phase III ordering in the disordered Phase II structure.

Table X-11. Infared and Raman frequencies of NH_4I.

		Thin Film Transmission*	Raman	Others	
NH_4I (Phase I) 300°K	$\nu_5(F_{1u})$	143 ± 1	(125)† (ν_5''?)		
NH_4I (Phase II) 240°K	$\nu_5(F_{1u})$	147 ± 1	(125)† (ν_5''?) (160)† (ν_5'?)		
NH_4I (Phase III) 100°K	$\nu_5(E_u, A_{2u})$	151 ± 1		135† 142†	145 neutron[17]
	$\nu_5'(E_g)$		155 ± 2	155	IR† & Raman[28]
	$\nu_5''(B_{2g})$		123 ± 2	123	IR† & Raman[28]
	$\nu_7'(E_g)$		57 ± 2	–	IR† & Raman[28]
	$\nu_7''(A_{1g})$		45 ± 2	–	IR† & Raman[28]
	$\nu_6'(E_g)$		283 ± 2	285 285 279	IR† & Raman[28] neutron[17] specific heat[31]

*Possibly Phase I at all temperatures (see Durig and Antion[28]).

†Broad, weak. May be multiphonon or the remains of ordering from Phase III, even though the crystal is in a disordered phase.

symmetries produced by the two electron-lattice interactions are identical. Consequently, both the transverse and longitudinal optic phonons corresponding to the reststrahlen mode should be Raman active. A band in NH_4Cl at 275 ± 5 cm^{-1} is observed at 80°K in the ordered phase, and corresponds quite will with the LO mode at 281 ± 5 cm^{-1} derived from the infrared reflection measurements. A weak broad mode at 225 ± 5 cm^{-1} in the NH_4Br Raman spectrum is also in agreement with the LO mode at 229 ± 5 cm^{-1} in the NH_4Br reflection results at 20°K. The electro-optic coupling coefficient in the ammonium halides that is responsible for this effect probably has the opposite sign from that present in CdS or CdSe where the LO mode observed in the Raman spectrum is an order of magnitude stronger than the corresponding TO mode.[30]

In summary, the external optical phonon modes in the ammonium chloride and bromide have been observed in all but the disordered NaCl phase. The number of modes and their symmetries agree with the group-theoretical predictions of the proposed structures. The temperature dependence of the frequencies and damping constants will allow future tests of theoretical models regarding overlap and anharmonic effect in the

interatomic forces when other independent low-temperature experimental parameters become available.

We would like to acknowledge the help and cooperation in this work of Professor C. W. Garland and Dr. N. Schumaker of the Department of Chemistry, M. I. T., and for supplying the single crystals of NH_4Cl and NH_4Br.

C. H. Perry, R. P. Lowndes

References

1. F. Simon, Ann. Physik 68, 241 (1922).
2. F. Simon and R. Bergmann, Z. Physik Chem. B8, 225 (1930).
3. K. Kamiyoshi, Sci. Res. Inst., Tohoku Univ. A8, 252 (1956).
4. Y. Sakamoto, J. Sci. Hiroshima Univ. A18, 95 (1954).
5. C. W. Garland and C. F. Yarnell, J. Chem. Phys. 44, 1112 (1966).
6. C. W. Garland and R. Renard, J. Chem. Phys. 44, 1130 (1966).
7. J. A. A. Ketalaar, Nature 134, 250 (1934).
8. V. Hori, K. Heiskanen, and M. Varteva, Ann. Acad. Scient. Fennicae AVI 144, 3 (1964).
9. H. A. Levy and S. W. Peterson, J. Am. Chem. Soc. 75, 1536 (1953).
10. A. Hettich, Z. Physik Chem. A168, 353 (1934).
11. R. Stevenson, J. Chem. Phys. 34, 1757 (1961).
12. E. L. Wagner and D. F. Hornig, J. Chem. Phys. 18, 296 (1950).
13. E. L. Wagner and D. F. Hornig, J. Chem. Phys. 18, 305 (1950).
14. W. Vedder and D. F. Hornig, J. Chem. Phys. 35, 1562 (1961).
15. A. D. B. Woods, B. N. Brockhouse, M. Sakamoto, and R. N. Sinclair, "Inelastic Scattering of Neutrons in Solids and Liquids," I. A. E. A., Vienna, p. 487, 1961.
16. H. Palevsky, J. Phys. Soc. Japan 17, Suppl. B-II, 367 (1962).
17. K. Mikke and A. Kroh, "Inelastic Scattering of Neutrons in Solids and Liquids," I. A. E. A., Vienna, p. 237, 1961.
18. A. C. Menzies and H. R. Mills, Proc. Roy. Soc. (London) 148A, 1107 (1935).
19. R. S. Krishnan, Proc. Indian Acad. Sci. A26, 432 (1947); A27, 321 (1948).
20. L. Couture and J. P. Mathieu, Proc. Ind. Acad. Sci. A28, 401 (1948).
21. L. Couture-Mathieu and J. P. Mathieu, J. Chem. Phys. 49, 226 (1952).
22. J. F. Reintjes, Jr., and C. H. Perry, Quarterly Progress Report No. 82, Research Laboratory of Electronics, M. I. T., July 15, 1966, pp. 48-53.
23. J. Z. Maze and C. H. Perry, Quarterly Progress Report No. 86, Research Laboratory of Electronics, M. I. T., July 15, 1967, pp. 41-51.
24. B. Szigetti, Proc. Roy. Soc. (London) A204, 51 (1950, 1951).
25. B. G. Dick and A. W. Overhauser, Phys. Rev. 112, 50 (1958).
26. C. H. Perry, R. Geick, and E. F. Young, Appl. Opt. 5, 1171 (1966).
27. R. S. Halford, J. Chem. Phys. 14, 8 (1946); D. F. Hornig, J. Chem. Phys. 16, 1063 (1948).

28. J. R. Durig and D. Antion (private communication, 1968).

29. R. Loudon, Advances in Physics, Vol. 13, p. 423, 1964.

30. J. F. Parrish, C. H. Perry, S. S. Mitra, O. Brafman, and I. F. Chang. Proc. II-VI Semi-Conductor Conference, edited by D. G. Thomas (Benjamin, New York, 1967, p. 1164.

31. C. C. Stephenson and H. E. Adams, J. Chem. Phys. 20, 1658 (1952).